

Article

An Eagle Strategy Arithmetic Optimization Algorithm for Frequency Stability Enhancement Considering High Renewable Power Penetration and Time-Varying Load

Ahmed. H. A. Elkasem ¹, Salah Kamel ¹, Mohamed H. Hassan ¹, Mohamed Khamies ¹
and Emad M. Ahmed ^{2,*}

¹ Department of Electrical Engineering, Faculty of Engineering, Aswan University, Aswan 81542, Egypt; ahmedhamdykasem2016@yahoo.com (A.H.A.E.); skamel@aswu.edu.eg (S.K.); mohamedhosnymoe@gmail.com (M.H.H.); mohamedahmedmak@yahoo.com (M.K.)

² Department of Electrical Engineering, College of Engineering, Jouf University, Sakaka 72388, Saudi Arabia

* Correspondence: emamahmoud@ju.edu.sa

Abstract: This study proposes a new optimization technique, known as the eagle strategy arithmetic optimization algorithm (ESAOA), to address the limitations of the original algorithm called arithmetic optimization algorithm (AOA). ESAOA is suggested to enhance the implementation of the original AOA. It includes an eagle strategy to avoid premature convergence and increase the populations' efficacy to reach the optimum solution. The improved algorithm is utilized to fine-tune the parameters of the fractional-order proportional-integral-derivative (FOPID) and the PID controllers for supporting the frequency stability of a hybrid two-area multi-sources power system. Here, each area composites a combination of conventional power plants (i.e., thermal-hydro-gas) and renewable energy sources (i.e., wind farm and solar farm). Furthermore, the superiority of the proposed algorithm has been validated based on 23 benchmark functions. Then, the superiority of the proposed FOPID-based ESAOA algorithm is verified through a comparison of its performance with other controller performances (i.e., PID-based AOA, PID-based ESAOA, and PID-based teaching learning-based optimization TLBO) under different operating conditions. Furthermore, the system nonlinearities, system uncertainties, high renewable power penetration, and control time delay has been considered to ensure the effectiveness of the proposed FOPID based on the ES-AOA algorithm. All simulation results elucidate that the domination in favor of the proposed FOPID-based ES-AOA algorithm in enhancing the frequency stability effectually will guarantee a reliable performance.

Keywords: load frequency control (LFC); arithmetic optimization algorithm (AOA); eagle strategy arithmetic optimization algorithm (ESAOA); proportional-integral-derivative (PID); fractional-order proportional-integral-derivative (FOPID); renewable energy sources (RESs); communication time delay



Citation: Elkasem, A.H.A.; Kamel, S.; Hassan, M.H.; Khamies, M.; Ahmed, E.M. An Eagle Strategy Arithmetic Optimization Algorithm for Frequency Stability Enhancement Considering High Renewable Power Penetration and Time-Varying Load. *Mathematics* **2022**, *10*, 854. <https://doi.org/10.3390/math10060854>

Academic Editors: Chuangyin Dang and Siyang Gao

Received: 8 January 2022

Accepted: 2 March 2022

Published: 8 March 2022

Publisher's Note: MDPI stays neutral with regard to jurisdictional claims in published maps and institutional affiliations.



Copyright: © 2022 by the authors. Licensee MDPI, Basel, Switzerland. This article is an open access article distributed under the terms and conditions of the Creative Commons Attribution (CC BY) license (<https://creativecommons.org/licenses/by/4.0/>).

1. Introduction

With the rapid growth of the global population, the establishment of new power plants becomes essential to supply all citizens' electrical requirements. Thus, energy planners are striving to devise a reliable design and a secure operation of these newly established power plants. Accordingly, the entities responsible for establishing new generation power plants are still intending to use renewable energy sources (RESs) instead of conventional power plants due to their good features (i.e., friendly to the environment, low cost, and abundant energy). However, with the rapid growth and use of RESs, the power system fluctuations increase due to the reduction of the system inertia [1,2]. Wherein, the power systems' operation and security will be affected according to those fluctuations. Additionally, the communication time delay in the controller action will affect the power system negatively, causing more fluctuations. Here, the optimal design and operation of electrical power grids are guaranteed when the different control loops are equipped, such as the primary control

loop and secondary or supplementary control loop. Both primary and supplementary control loops are responsible for regulating the power system frequency to the scheduled value. The role of the primary control loop is to dampen out the small deviations of system frequency in normal conditions [3]. The main objective of load frequency control (LFC) in multi-area interconnected power grids is to keep the frequency of each area in pre-specified tolerance and the tie-line power flows within limits without bulky complications in the electrical system. The strategy behavior of LFC is monitoring the area-frequency and the tie-line power flows, and then it computes the net required change in power generation to meet these changes. The changes in area-frequency and tie-line power flows are represented by area control error that needs to be corrected by adjusting the MW outputs of generators to accommodate perturbing load demands [4].

Due to the complexity of the new power grids' structure, the oscillation in the system may spread to wide inter-connected areas causing partial or total system blackouts. The issue of the LFC problem has been tackled by implementing various control techniques. In this regard, intelligence control techniques were utilized to maintain system stability, through fuzzy logic controllers [5], artificial neural networks [6], and adaptive neuro-fuzzy controllers [7]. In addition, the issue of LFC has been solved through the implementation of several robust control methods, such as the H-infinite technique [8] and μ -synthesis [9]. Furthermore, the frequency stability has been achieved to be within tolerable limits, utilizing optimal control techniques, such as the linear quadratic regulator [10] and linear quadratic gaussian [11]. However, the aforementioned control techniques are sufficient and apt to overcome LFC issues. However, they are dependent on the expertise of the designer, testing, and trial and error methods in selecting the controller parameters which take a long time to adjust and estimate the parameters of the considered controllers. On the other hand, the proportional-integral-derivative (PID) is still the best choice in stabilizing power systems owing to its reputable merits (i.e., simple in construction and requiring less cost compared to other controllers). However, during abnormal conditions, the PID controller did not give the desired performance as it is susceptible to system uncertainties. Therefore, it is necessary to fine-tune the PID controller parameters to face any distortion of the system.

In this regard, different optimization techniques are utilized to fine-tune the PID controller parameters for solving the problem of PID controller sensitivity. Firstly, the authors applied traditional methods for adjusting and selecting PID controller parameters, such as the tracking approach [12], aggregation methods [13], and interior-point algorithm [14]. These techniques suffer from some obstacles (i.e., slump, deathtrap in local minimums, needing more iterations, and depending on their initial conditions) to achieve the desired target. According to the difficulties of the traditional algorithms, meta-heuristic optimization techniques are implemented to help the designers to design optimal controllers to maintain the stability of the power grids. Meta-heuristic optimization techniques were not the only techniques implemented to stabilize the power system frequency; artificial bee colony [15], salp swarm algorithm [16], and whale optimization algorithm [17] were also utilized. Although these techniques perform their role in ensuring the effective LFC design, they suffer from some shortcomings, such as slowing in the rate of convergence, poor local search capability, and local optimum convergence. Thus, many mathematical studies have been conducted to develop more algorithms by improving previous methods to overcome the mentioned shortcomings. In this regard, several improved algorithms have been implemented, such as improved stochastic fractal search algorithm [18] and sine augmented scaled sine cosine [19]. According to this motivation, this study proposes a novel improved algorithm derived from the arithmetic optimization algorithm (AOA), which is called ESAOA to select the optimum PID controller parameters in the secondary control loop.

On the other side, the fractional-order controllers (FOCs) have become a distinct candidate in power system stabilizing due to their advantages (i.e., flexibility in configuration and a higher degree of freedom). The FOCs have several types of poles, such as the hyper-

damped poles, that need to be fine-tuned. Accordingly, this leads to expansion in the stable region, giving more flexibility in the controller design process [20]. Furthermore, there are several types of controllers belonging to the FOCs' family, and the fractional-order PID (FOPID) is one of this family that has been presented in [21]. According to the advantages of the FOPID controller, it has been implemented in this work and has been optimized utilizing the improved ESAOA algorithm.

Recently, the AOA technique has been proposed as a new meta-heuristic algorithm by Albualigah et al. in 2020. Foremost, the formulation of the AOA technique is based on arithmetic as it represents one of the main aspects of number theory in mathematics. In this optimization algorithm, the main operators in mathematics (i.e., multiplication, division, subtraction, and addition) are utilized as the extensive coverage process of the search space using agents. According to the arithmetic operators, the multiplication process and division process are represented as the two candidates to complete the exploration search mechanism according to the highly distributed values of these two operators. As for the exploitation search mechanism, the subtraction operator and addition operator have performed this mechanism according to their merits (i.e., results with high-dense). The haste of choosing the AOA over other techniques returns to the major benefits of AOA (i.e., has a gradient-free mechanism and reaches the global solution with a few search agents). In addition, the AOA is a reputable algorithm that provides promising results in solving different engineering designs [22]. AOA is utilized to solve different mechanical engineering designs problems such as design of welded beam, design of pressure vessel, and design of compression spring [23]. It has also been applied in the civil engineering field in the steel structures for buildings with improving the proposed technique to gain an update in the searching process [24]. In [25], the AOA was improved to solve one of the automotive engineering field problems (i.e., planning the robot path). In addition, the improved AOA has been applied in the design of combined cooling, heating, and power systems for saving energy [26]. Furthermore, AOA has been proposed to evaluate images of COVID-19 in the medical field with distinguished results [27]. Accordingly, the first utilizing of the AOA in regard to solving the LFC issue is in [28], by considering RESs penetrated in two-area multi-sources and it has a superiority to overcome all oscillations compared to other utilized techniques. Researchers are still applying the AOA in a variety of engineering problems, medical field problems, and different life problems by improving the exploration and exploitation processes to gain an improved technique that relies on AOA achieving promising results. In this regard, this work proposes an improved technique known as ESAOA for stabilizing the power system frequency with different challenges in the power system.

On the other hand, another classification of the LFC issue depends on several scientific studies that have been conducted on several electrical power systems (i.e., single-area power system, two-area power system, three-area power system, and four-area power system). For a single area, the problem of LFC is tackled and presented in [29–33]. In addition, the frequency stability of two-area interconnected power plants is investigated in [34–38]. Additionally, many studies have been presented on solving the LFC problem by considering three-area interconnected power plants [39,40]. Furthermore, many researchers have studied the LFC issue according to four-area interconnected power plants [41,42]. Researchers are still studying the issue of the LFC problem with various configurations of power systems using different proposed controllers adjusted with different recent algorithms to gain more system stability.

Concerning the LFC problem, the aforementioned studies in the literature review with all their controller design processes highlight the issues of stabilizing the system frequency under numerous challenges. Conversely, several studies cope with the frequency stabilizing issue utilizing conventional techniques to obtain the controller parameters values. Even so, these conventional techniques suffer from the slump, deathtrap in local minimums, requiring more iteration to gain the best solution, and depending on their initial conditions. Thus, this study proposed a recently improved meta-heuristic known as ESAOA that was selected

meticulously according to its merits (i.e., develop the searching process and gain the global solution with a few search agents). Several researchers include multi-area interconnected systems with each area included by only one generation unit [37,39]. In contrast, this paper studied a two-area interconnected system considering three-generation units in each area (i.e., thermal, hydro, and gas). Furthermore, several studies do not take into consideration the effect of RESs penetration in the studied system amalgamation with other conventional sources [41,42]. In this study, the effect of high RESs penetration has been taken into account (6% wind energy in the first area –3% PV energy in the second area) as the whole world moves towards using RESs with conventional power plants. Moreover, the communication time delay is taken into consideration in this study as before and after the proposed control action to endorse the effectiveness of the proposed technique. To increase challenges in the studied system, various types of load variations have been applied (i.e., Step Load Perturbation (SLP), series SLP, and random variation) to elucidate the superiority of the proposed controller using the proposed technique in getting the system frequency within tolerable limits.

This study tries to overcome the limitations of previous studies. Table 1 outlines the difference between this study and other previous studies related to loading frequency control.

Additionally, the crucial contributions of this work can be depicted as:

- Proposing a new improved algorithm called ESAOA to develop the strategy of exploration and exploitation of the AOA technique.
- Comparing the performance of the ESAOA algorithm with other algorithms considering 23 benchmark functions.
- Applying the ESAOA to select the optimal parameters of FOPID and PID controllers in hybrid two-area power systems.
- Comparing the performance of the improved ESAOA-based FOPID controller with different techniques, i.e., teaching learning-based optimization (TLBO)-, AOA-, and ESAOA-based PID controller to enhance the studied system performance.
- Considering various types of load variations (i.e., SLP, series SLP, and random load variation) to test the validity of the proposed controller using the proposed technique in regulating the studied system frequency.
- Considering the high penetration of RESs emerging in both areas of the studied power system when adjusting the controller parameters to achieve system stability.
- Considering communication time delay in both areas as a challenge to evaluate the robustness of the obtained FOPID controller parameters using the proposed modified technique.

The remainder of this manuscript is organized in sections that are mentioned as follows: the studied system under investigation which considers penetration of RESs is illustrated in Section 2. Section 3 discusses the proposed FOPID and PID controller's approaches and the formulation of the studied problem besides to discussing the procedure of the modified ESAOA technique. Moreover, the simulation results according to different scenarios are clarified in Section 4. Finally, Section 5 summarizes the conclusions of the current work.

Table 1. Comparison between the motivation of current work and other published works.

References	Proportional-Integral-Derivative Controllers Structure	Controller Design Adoption	Step Load Perturbation (SLP) Challenge	Type of Proposed System	Penetration of Renewable Energy Sources (RESs)	Communication Time Delay
[29]	(PID)/PI	Firefly algorithm (FA)	SLP	Single	Not considered	Not considered
[30]	PID	Elephant herding optimization (EHO)	SLP	Single	Not considered	Not considered
[31]	PID	Linearization system modeling requirement theory	SLP	Single	Not considered	Not considered
[32]	PID	Ant colony optimization technique (ACOT)	SLP	Single	Not considered	Not considered
[34]	I/PI	Grey wolf optimizer (GWO)	SLP	Multi	Considered with low penetration	Not considered
[35]	I/PI	Sine cosine algorithm (SCA)	SLP	Multi	Considered with low penetration	Not considered
[36]	I/PI	Harris hawks algorithm (HHA)	SLP	Multi	Considered with low penetration	Not considered
[37]	PID	Analytic hierarchy process (AHP)	SLP	Multi	Not considered	Not considered
[39]	PI/PID	Backtracking search algorithm (BSA)	SLP/random load variation	Multi	Not considered	Not considered
[40]	PID	Flower pollination algorithm (FPA)	SLP	Multi	Not considered	Not considered
[42]	PI/PID	Grey wolf optimization (GWO)	SLP	Multi	Not considered	Not considered
This study	PID	Eagle strategy arithmetic optimization algorithm (ESAOA)	SLP/series SLP/random load variation	Multi	Considered with high penetration at both areas	Considered before and after the controller action

2. The Studied Power Grid

2.1. Configuration of a Two-Area Interconnected Power Grid

This section introduces the construction of the studied two-area interconnected power plant in detail. Where the investigated power plant consists of two distinct areas labeled area-1 and area-2. Furthermore, each area is included by a variety of conventional power plants (i.e., reheat thermal power plant, hydropower plant, and gas turbine) that are connected totally with each other. Each area has a capacity with a rated power of 2000 MW [43]. Furthermore, the thermal power plant contributes 1087 MW, the hydropower plant contributes 653 MW, and the gas turbine contributes 262 MW [43]. For more details, Figure 1 illustrates the structure of the studied power plant. In addition, Figure 2 describes the model of the studied interconnected two-area power plant. Figure 2 includes symbols that need to be known to complete the process of LFC, such as the frequency bias factor of the i_{th} area (B_i) being equal to 0.425 (p.u.M.W/Hz) for both areas. The synchronizing coefficient between both areas is denoted by (T_{12}), which equal to 0.0433 (p.u.M.W/Hz). The frequency oscillation and load perturbation in the i_{th} area are described as Δf_i (Hz) and ΔP_{D_i} (p.u.M.W), respectively. The speed regulation of each unit of the i_{th} area is denoted by (R_i), equaling to 2.4 (Hz/p.u.M.W). The parameters of all transfer functions of all conventional generation units are mentioned in [28]. The tie-line power exchange between both areas is described as the power transferred from area-1 to area-2 and power transmitted from area-2 to area-1 are (ΔP_{tie1-2}) and (ΔP_{tie2-1}), respectively. Furthermore, the proposed FOPID and PID controllers utilizing modified ESAOA is equipped in each area of the proposed studied system for each generation unit to overcome the oscillation of frequency in both areas and tie-line power between them by extracting more active power. The input signal of the proposed FOPID and PID controllers is the area control area (ACE), which consists of ΔP_{tie} plus $B_i \times \Delta f_i$, while the output signal represents the action of the secondary controller to generate extra active power for stabilizing the power system frequency. Furthermore, the ACEs of both areas can be expressed as follows:

$$ACE_1 = \Delta P_{tie1-2} + B_1 \Delta f_1 \tag{1}$$

$$ACE_2 = \Delta P_{tie2-1} + B_2 \Delta f_2. \tag{2}$$

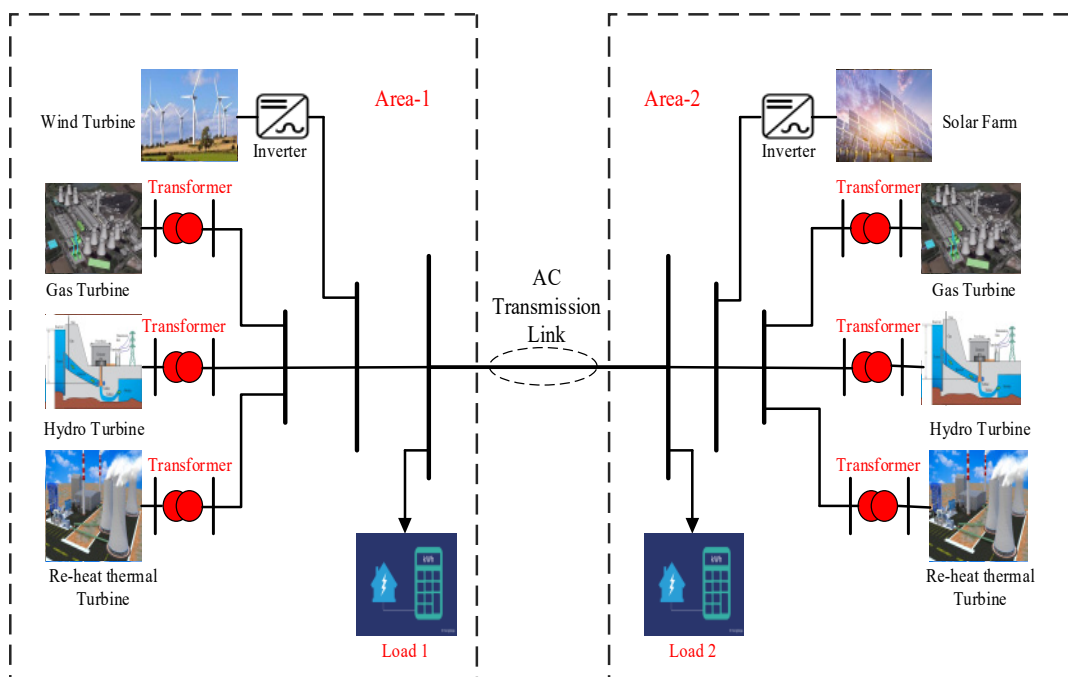


Figure 1. The structure of the studied two-area interconnected power grid.

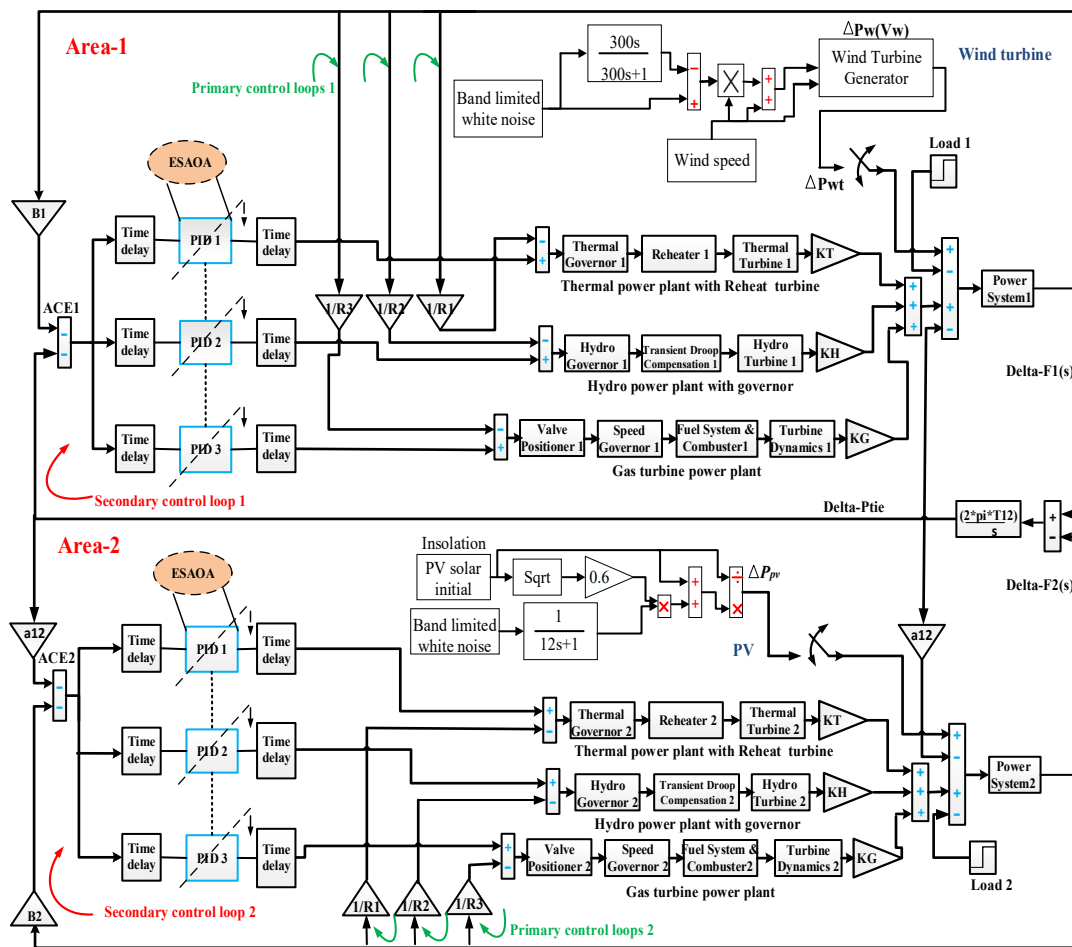


Figure 2. The transfer functions of the studied two-area interconnected power grid.

2.2. The Configuration of a Wind Power Model

This section introduces a simplified model of a wind power generating system, where the considered model was built using the MATLAB/SIMULINK program for attaining the oscillations generated by wind turbines as shown in Figure 3 [44]. The white noise block is utilized to achieve a random wind speed. This random wind speed signal is multiplied by the real wind speed to obtain the resulting signal, which represents the input to the wind turbine generator. Here, the input signal to the wind turbine generator is responsible for obtaining random wind output power oscillations. The captured output power of the wind turbine can be illustrated in the subsequent equations [44]:

$$P_{wt} = \frac{1}{2} \rho A_T v_w^3 C_p(\lambda, \beta) \tag{3}$$

$$C_p(\lambda, \beta) = C_1 \left(\frac{C_2}{\lambda_i} - C_3 \beta - C_4 \beta^2 - C_5 \right) \times e^{-\frac{C_6}{\lambda_i}} + C_7 \lambda_T \tag{4}$$

$$\lambda_T = \lambda_T^{OP} = \frac{\omega_T r_T}{V_W} \tag{5}$$

$$\frac{1}{\lambda_i} = \frac{1}{\lambda_T + 0.08\beta} - \frac{0.035}{\beta^3 + 1} \tag{6}$$

Here, P_{wt} represents the output power of the wind turbine that penetrated in area-1, A_T signifies the rotor swept area in m^2 , ρ signifies the air density (nominally 1.22 kg/m^3), V_W represents the rated wind speed in m/s , C_1 – C_7 represents the turbine coefficients, β signifies the pitch angle, λ_T refers to the appertains optimally to the tip-speed ratio

(TSR), (r_T) represents the blade length of the rotor radius, and λ_i refers to the intermittent TSR [45]. In addition, Table 2 displays the wind turbine parameters. Additionally, the output generated power from the wind turbine is 134 MW, which is obtained by an amalgamation of 178 wind turbines of 0.75 MW per wind turbine. Figure 4 shows the random output power of wind energy.

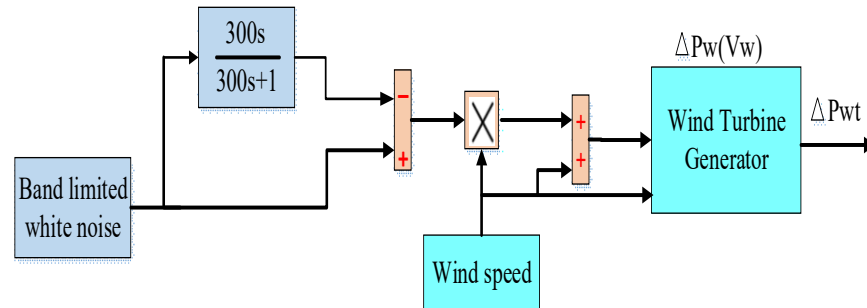


Figure 3. The wind power modeling using MATLAB/Simulink [44].

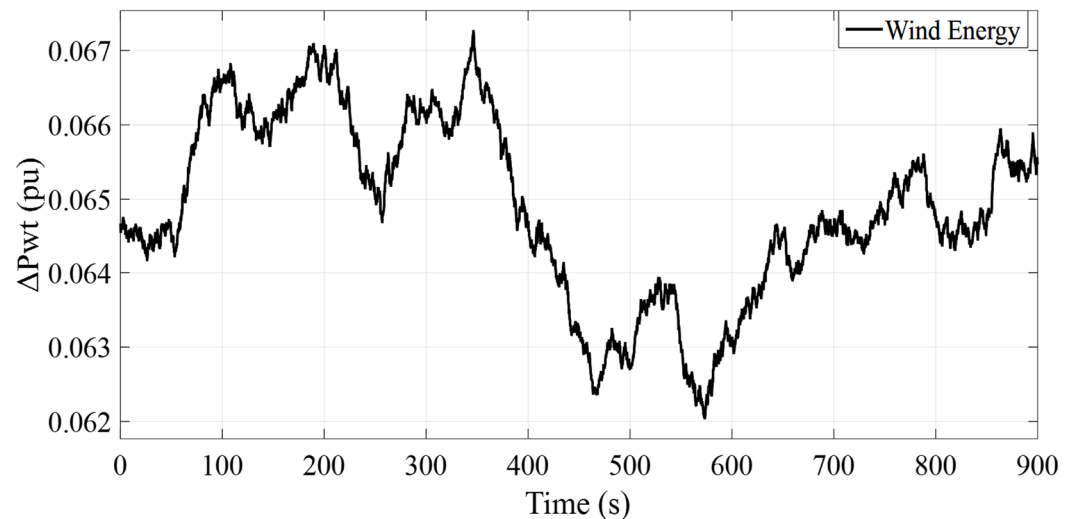


Figure 4. The output power from the wind power model.

Table 2. The nominal parameters of the wind farm [44].

Parameters	Values
P_{wt}	750 KW
V_W	15 m/s
A_T	1648 m ²
r_T	22.9 m
ω_T	22.5 rpm
C_1	-0.6175
C_2	116
C_3	0.4
C_4	0
C_5	5
C_6	21
C_7	0.1405

2.3. The Configuration of PV Model

This section introduces the model of solar energy, which is used to generate the output power. Furthermore, Figure 5 describes the model of generated power from the solar farm. The random output oscillations are achieved in this model through a white noise block

that is multiplied by the standard power deviation value generated from a real PV plant. The generated solar energy deviation is much like the changing of real power energy as follows [44]:

$$\Delta P_{solar} = 0.6 \times \sqrt{P_{solar}} \tag{7}$$

Here, P_{solar} represents the standardized output power generated from a real solar farm and the deviation of generated solar energy can be represented in ΔP_{solar} term. The generated solar energy that penetrated the studied power system is 60 MW (3% of the total power capacity). Figure 6 clears the output power from the considered solar farm model.

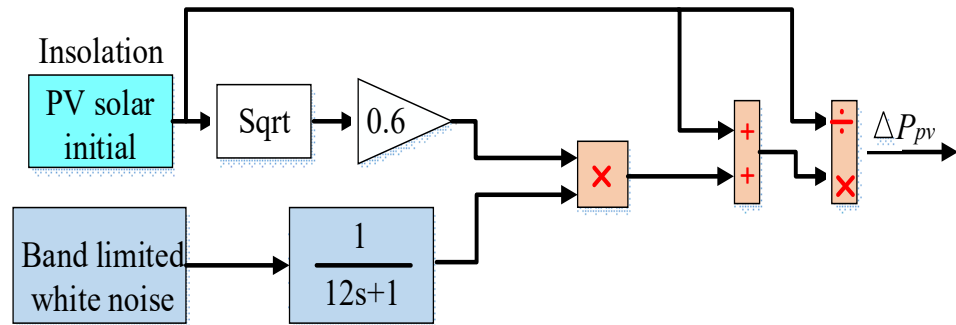


Figure 5. The solar energy modeling using MATLAB/Simulink [44].

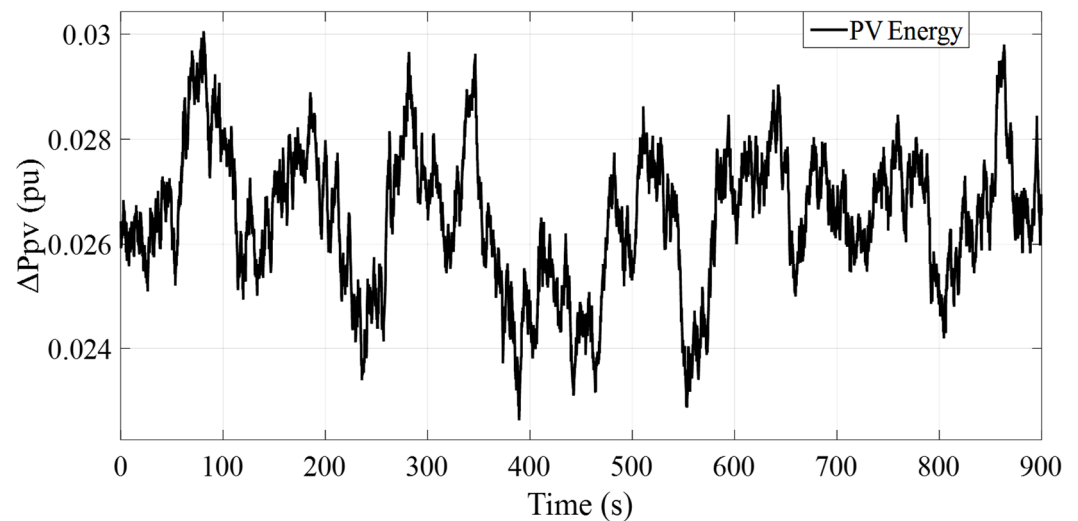


Figure 6. The output PV power.

3. The Proposed Control Strategy

3.1. The Proposed Algorithm

3.1.1. Arithmetic Optimization Algorithm (AOA)

The original AOA algorithm is a metaheuristic optimization algorithm, which is proposed in [22]. This algorithm employs the distribution behavior of the principal arithmetic operators in the calculation such as multiplication (M), division (D), addition (A), and subtraction (S). The AOA algorithm uses the math optimizer accelerated (MOA) function to choose between the exploration and exploitation search phase. The MOA function can be provided as follows:

$$MOA(iter) = Min + iter \times \left(\frac{Max - Min}{Max_iter} \right) \tag{8}$$

where, $iter$ is the current iteration, Max_iter denotes the maximum number of iterations, Max and Min are the maximum and minimum values of the accelerated function, respectively.

(a) Exploration phase

Figure 7 shows the model updating the position of the math operators in the original AOA algorithm towards the optimum area. In the exploration phase, the AOA algorithm uses two principal strategies, the multiplication (M) search strategy and the division (D) search strategy, to find the better solution. The new position updating equation for the exploration phase is calculated from the following equation:

$$x_{i,j}(iter + 1) = \begin{cases} best(x_j) \div (MOP + \epsilon) \times ((ub_j - lb_j) \times \mu + lb_j), & r2 < 0.5 \\ best(x_j) \times MOP \times ((ub_j - lb_j) \times \mu + lb_j), & otherwise \end{cases} \quad (9)$$

where $x_{i,j}(iter + 1)$ is the j th position of the i th solution at the current iteration, and $best(x_j)$ denotes the j th position in the best-achieved solution so far. μ denotes the control parameter. MOP is the math optimizer probability which can be calculated as follows:

$$MOP(iter) = 1 - \frac{iter^{\frac{1}{\alpha}}}{Max_iter^{\frac{1}{\alpha}}} \quad (10)$$

where, α denotes a sensitive parameter.

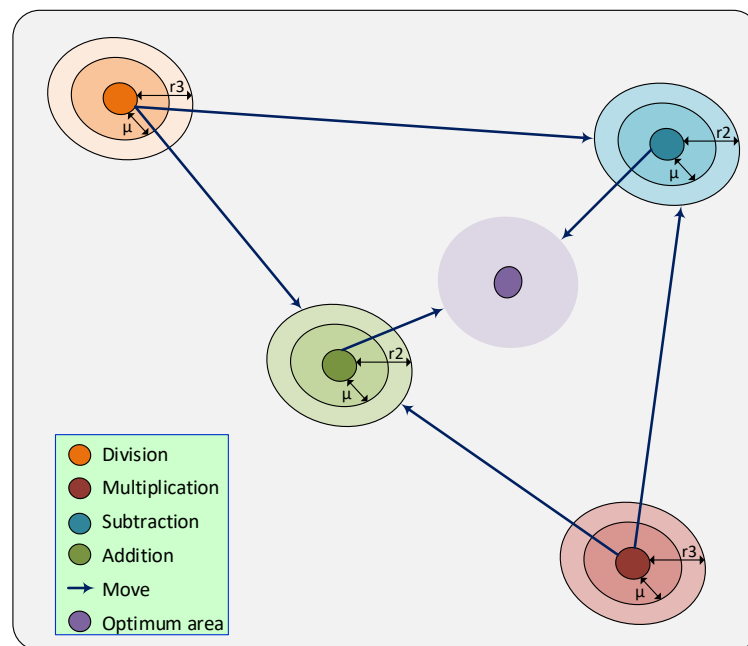


Figure 7. Model of updating the position of math operators in the original AOA algorithm towards the optimum area.

(b) Exploitation phase

In the exploitation phase, the AOA algorithm uses the two principal strategies that are the subtraction (S) search strategy and the addition (D) search strategy to gain the high-dense solutions:

$$x_{i,j}(iter + 1) = \begin{cases} best(x_j) - MOP \times ((ub_j - lb_j) \times \mu + lb_j), & r2 < 0.5 \\ best(x_j) + MOP \times ((ub_j - lb_j) \times \mu + lb_j), & otherwise \end{cases} \quad (11)$$

3.1.2. The Proposed Eagle Strategy Arithmetic Optimization Algorithm (ESAOA)

The Eagle strategy is proposed and developed by Yang et al. [46]. This strategy is utilized to develop many algorithms to solve real-world optimization problems such as parameters identification of photovoltaic models [47,48], power loss minimization [49],

optimal placement of distribution generation in micro-grid [50], Quality of service (QoS)-aware cloud service composition [51]. This strategy is inspired by foraging the eagle’s behavior, which flies randomly in analogy to the Levy flights. It is the two-phase method: global search randomization phase and an intensive local search [49]. The first phase targets essentially to examine the search space globally and quickly find a promising solution, while the goal of the second stage is to find the best solution through generating an intensive local search based on the attained solution in the first phase. The advantage of this strategy is that there is no limit to the kinds of techniques used in each phase. Any algorithm that can flexibly reach better results was used in any phase [49].

The flowchart of the proposed ESAOA algorithm is shown in Figure 8. During the iteration of the proposed algorithm, the new position can be generated by a Levy flight as shown in the following equation:

$$x_{i,j}(iter + 1) = x_{i,j}(iter) - \gamma(x_{i,j}(iter) - best(x_j)) \oplus Levy(\lambda) \tag{12}$$

$$x_{i,j}(iter + 1) = x_{i,j}(iter) + \frac{0.01u}{|v|^{1/\lambda}}(x_{i,j}(iter) - best(x_j)) \tag{13}$$

where γ denotes the step scaling size, \oplus is the process of element-wise multiplications, λ refers to the Levy flight exponent, while u and v is expressed as follows:

$$u \sim N(0, \sigma_u^2), v \sim N(0, \sigma_v^2). \tag{14}$$

The standard deviations σ_u and σ_v can be explained as:

$$\sigma_u = \left[\frac{\sin\left(\frac{\lambda\pi}{2}\right) \cdot \Gamma(1 + \lambda)}{2^{(\lambda-1)} \lambda \cdot \Gamma\left(\frac{1+\lambda}{2}\right)} \right]^{1/\lambda}, \sigma_v = 1 \tag{15}$$

where Γ denotes the Gamma function.

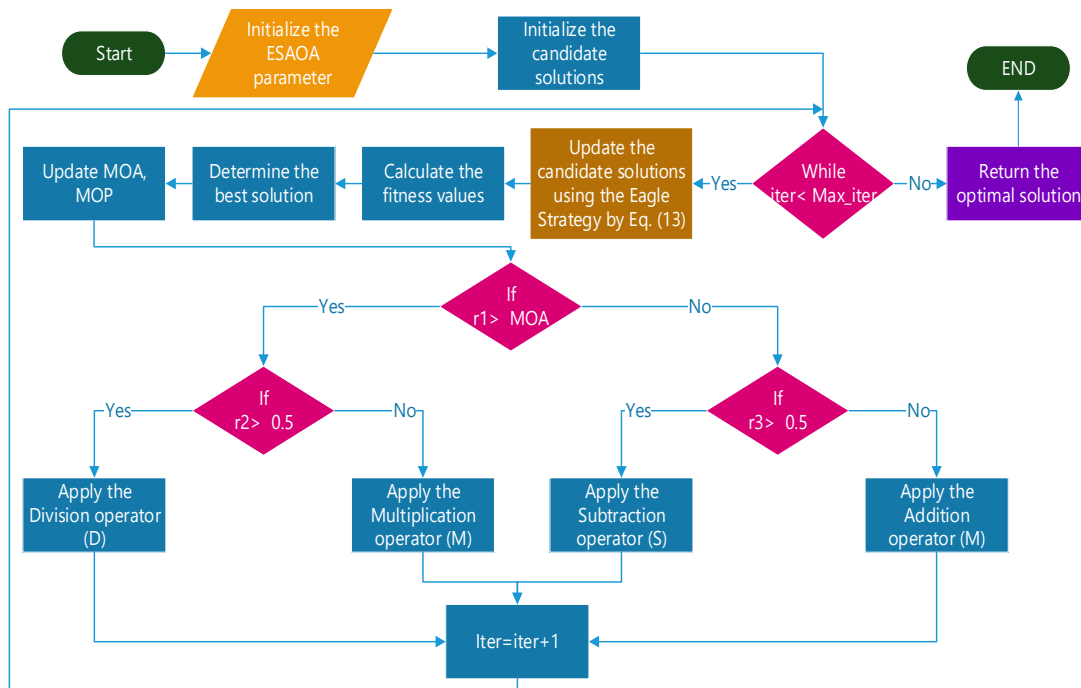


Figure 8. Flowchart of the proposed ESAOA technique.

3.2. The Proposed Controller

3.2.1. The Proportional-Integral-Derivative (PID)

The construction of the PID controller is shown in Figure 9 and mathematically mentioned in Equation (16). In general, the PID controller depends on three basic terms, known as the proportional gain ($k_{p(pid)}$), the integral gain ($k_{i(pid)}$), and derivative gain ($k_{d(pid)}$). Where each term has an important role, the proportional term can stabilize the gain values, however, it produces a steady-state error in its response, the integral term can eliminate the steady-state error effectively, and the derivative term can reduce the rate of change of error [40]. The main target of the proposed PID controller is to maintain the system frequency and the tie-line power deviations of the studied system within tolerable limits. During normal conditions, each area in the multi-interconnected power system can handle its connected loads and keeps all system parameters within specified limits. However, during abnormal conditions in any area of multi-interconnected power systems, the stability of the power grid is affected badly. Thus, the LFC is committed to overcoming these oscillations and returning the system frequency as well as the tie-line power flow to their stable conditions:

$$PID(s) = k_{p,i(pid)} + \frac{K_{i,i(pid)}}{s} + K_{d,i(pid)}s. \tag{16}$$

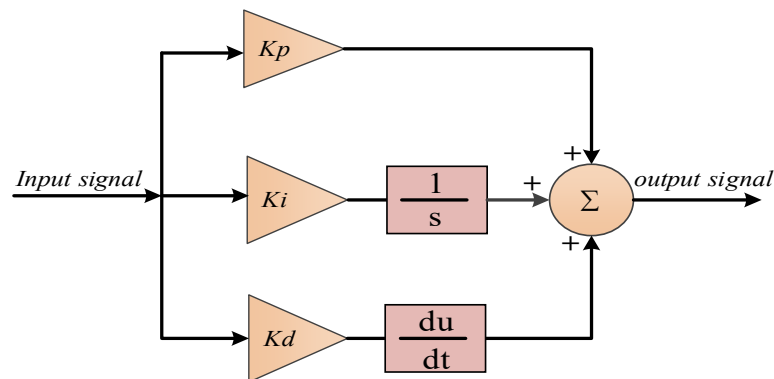


Figure 9. The structure of the PID controller.

The studied power grid consists of two interconnected areas. Where each area is equipped with three-generation units (i.e., thermal, hydro, and gas). Furthermore, each generation unit has been preceded by a PID controller for adjusting the frequency deviations of each unit. The constraints of gain values, $k_{p(pid)}$, $k_{i(pid)}$, and $k_{d(pid)}$ utilized in this study in both areas of the studied power grid are expressed as follows:

$$k_{p,i(pid)}^{max} \geq k_{p,i(pid)} \geq k_{p,i(pid)}^{min} \tag{17}$$

$$k_{i,i(pid)}^{max} \geq k_{i,i(pid)} \geq k_{i,i(pid)}^{min} \tag{18}$$

$$k_{d,i(pid)}^{max} \geq k_{d,i(pid)} \geq k_{d,i(pid)}^{min} \tag{19}$$

where; $k_{p,i(pid)}^{min}$, $k_{i,i(pid)}^{min}$, $k_{d,i(pid)}^{min}$, $k_{p,i(pid)}^{max}$, $k_{i,i(pid)}^{max}$, and $k_{d,i(pid)}^{max}$ represent the minimum and maximum PID controller parameter values, respectively. The i represents the specified controller related to the three-generation units in the proposed studied system ($i = 1, 2, 3$). Moreover, the constraints of the proposed PID controller parameters are in the [0, 10] period.

3.2.2. The Fractional-Order Proportional-Integral-Derivative (FOPID)

The concept of the fractional order in the design process related to the PID controller is proposed by Podlubny [52,53]. Whereas, the main difference between the FOPID controller and the PID controller is that, the order of integral and derivative of the FOPID controller

is not an integer. As a result, this characteristic leads to providing extra degrees of freedom in tuning the controller as well as maintaining a more dynamic performance compared to a conventional PID controller. Thus, the FOPID controller is implemented for solving the LFC problem in different constructions of a power system [54,55]. Figure 10 depicts the general form of the FOPID controller and is mathematically mentioned as:

$$PI^\lambda D^\mu(s) = k_{p,i(FOPid)} + \frac{K_{i,i(FOPid)}}{s^\lambda} + K_{d,i(FOPid)}s^\mu. \tag{20}$$

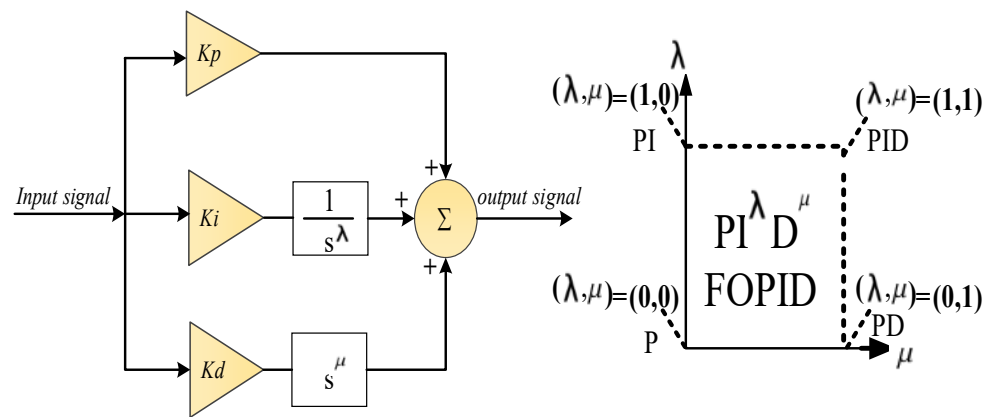


Figure 10. The structure of the FOPID controller.

In Equation (20), $k_{p(FOPid)}$, $k_{i(FOPid)}$, and $k_{d(FOPid)}$ are represented as the proportional, integral, and derivative gains of the FOPID controller. Where the constraints of the P term, I term, and D term in the FOPID controller parameters are in the range of (0, 10). Furthermore, λ and μ denote the fractional order operators, which are often adjustable in the range of (0, 1). As depicted in Figure 10, the FOPID controller performs much like different models of a simple PID construction by selecting zero and one for λ and μ . The constraints of gain values, $k_{p(FOPid)}$, $k_{i(FOPid)}$, $k_{d(FOPid)}$, λ , and μ utilized in the studied power grid are expressed as follows:

$$k_{p,i(FOPid)}^{max} \geq k_{p,i(FOPid)} \geq k_{p,i(FOPid)}^{min} \tag{21}$$

$$k_{i,i(FOPid)}^{max} \geq k_{i,i(FOPid)} \geq k_{i,i(FOPid)}^{min} \tag{22}$$

$$k_{d,i(FOPid)}^{max} \geq k_{d,i(FOPid)} \geq k_{d,i(FOPid)}^{min} \tag{23}$$

$$\lambda_{i^{max}} \geq \lambda_i \geq \lambda_{i^{min}} \tag{24}$$

$$\mu_{i^{max}} \geq \mu_i \geq \mu_{i^{min}} \tag{25}$$

where $k_{p,i(FOPid)}^{min}$, $k_{i,i(FOPid)}^{min}$, $k_{d,i(FOPid)}^{min}$, $\lambda_{i^{min}}$, $\mu_{i^{min}}$, $k_{p,i(FOPid)}^{max}$, $k_{i,i(FOPid)}^{max}$, $k_{d,i(FOPid)}^{max}$, $\lambda_{i^{max}}$, and $\mu_{i^{max}}$ represent the minimum and maximum FOPID controller parameter values, respectively.

In the control designing process, four popular kinds of performance criteria are known as integral time absolute error (ITAE), integral of squared error (ISE), integral time squared error (ITSE), and integral of absolute error (IAE). According to the good performance of ISE and ITAE criteria, these are often utilized in literature to minimize the objective function compared to the ITSE and IAE criteria. The role of ISE encompasses the integration of the square error over time. ISE can threaten/penalize the large errors compared to small errors as the square of the large errors will be much larger than those small errors. Thus, the ISE is selected to minimize larger errors quickly by tolerating continuous small errors over time. This will lead to quick responses in penalizing the large errors, however with oscillations from small errors. Accordingly, the ITAE becomes a strong candidate for minimizing the

objective function in this work due to its integrating process of the absolute error multiplied by time over time. For ease, it has an additional time that is multiplied by the error for making the system faster than using other objective function criteria. It can be said that the *ITAE* tuning can achieve system settle more quickly than *ISE* tuning [56]. Thus, the authors in this work applied the integral time absolute error (*ITAE*) to minimize the studied objective function to obtain the optimal system performance. The expression of *ITAE* is expressed as follows:

$$J = ITAE = \int_0^{Tsim} t \cdot [|\Delta f_1| + |\Delta f_2| + |\Delta p_{tie}|] \cdot dt. \tag{26}$$

Here, *J* is the objective function needing to be minimized through the controller action, *Tsim* represents the total simulation time of the optimization process, and *dt* represents a given time interval for taking samples along the simulation process.

3.3. The Procedure of the ESAOA Algorithm

In this section, the supremacy of the proposed ESAOA algorithm is confirmed by 23 benchmark functions. The investigation of these benchmark functions is executed by MATLAB (R2020a) on a computer with an 8 GB RAM environment and with Intel(R) Core (TM) i5-9400F CPU 2.90 GHz (Intel Corporation, Mountain View, CA, USA).

Benchmark Functions

In this subsection, the effectiveness and accuracy of the proposed ESAOA technique are evaluated on 23 benchmark functions for the results achieved by using the conventional AOA technique and three recent optimization algorithms, the grey wolf optimizer (GWO) [57], the tunicate swarm algorithm (TSA) [58], and the seagull optimization algorithm [59]. The control parameter of the proposed and other algorithms are illustrated in detail in Table 3.

Table 3. The control parameters of the proposed and other techniques.

The Control Parameter	Algorithms
Number of population size = 50 Iterations number = 200 Number of runs = 20	Common parameters
$\alpha = 5; \mu = 0.5$ (Default)	ESAOA AOA
Convergence parameter (<i>a</i>) linear reduction from 2 to 0 (Default) Pmin = 1; Pmax = 4 (Default)	GWO TSA
Control Parameter (A) linear reduction from 2 to 0; <i>fc</i> = 2 (Default)	SOA

The solutions of the proposed ESAOA algorithm are compared with these recent techniques in Table 4. All these algorithms have been implemented for a population size of 50 and the maximum number of iterations is 200 for 20 independent runs. The qualitative metrics using the proposed ESAOA algorithm for 9 benchmark functions including 2D views of the functions, search history, average fitness history, and convergence curve are displayed in Figure 11.

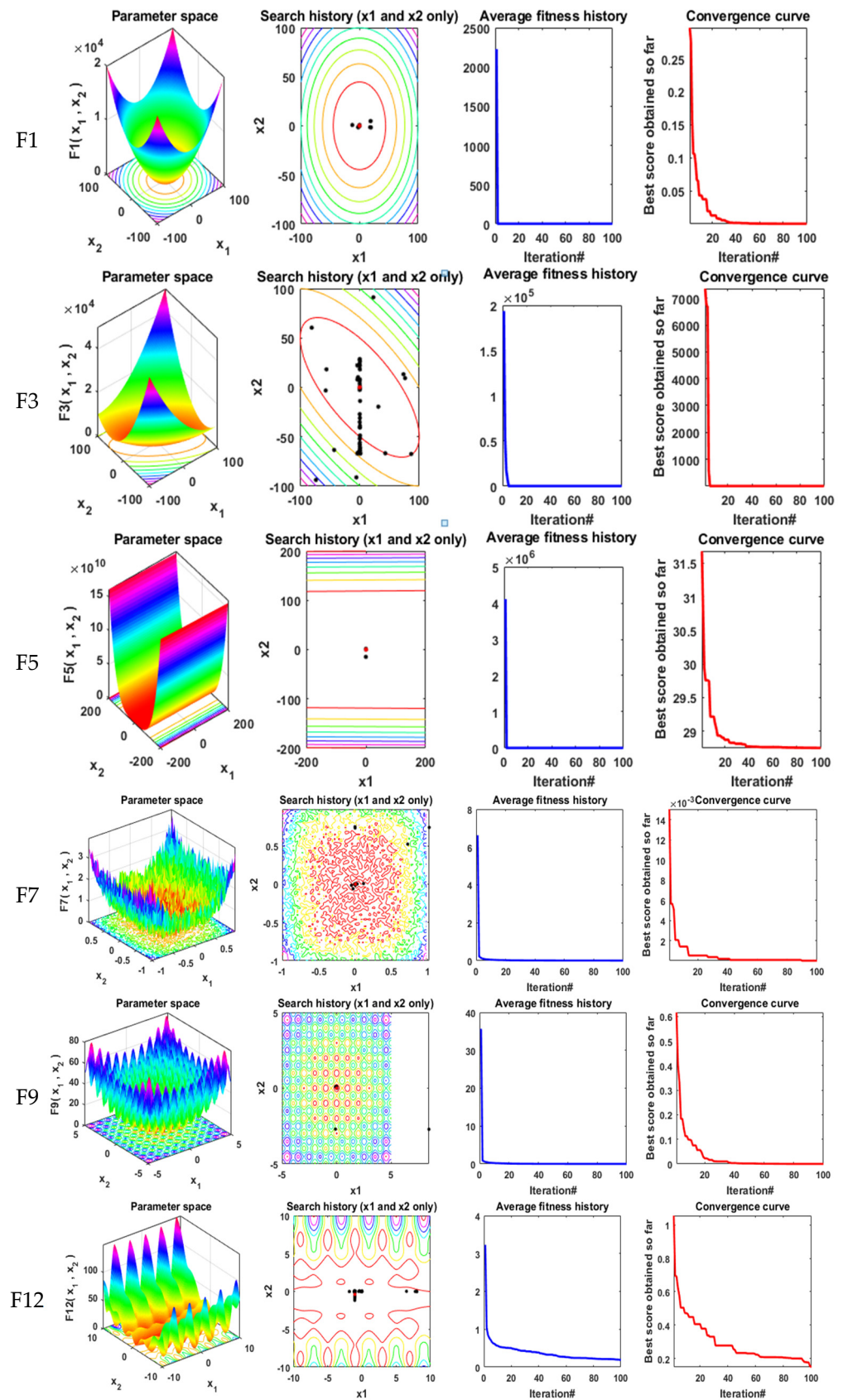


Figure 11. Cont.

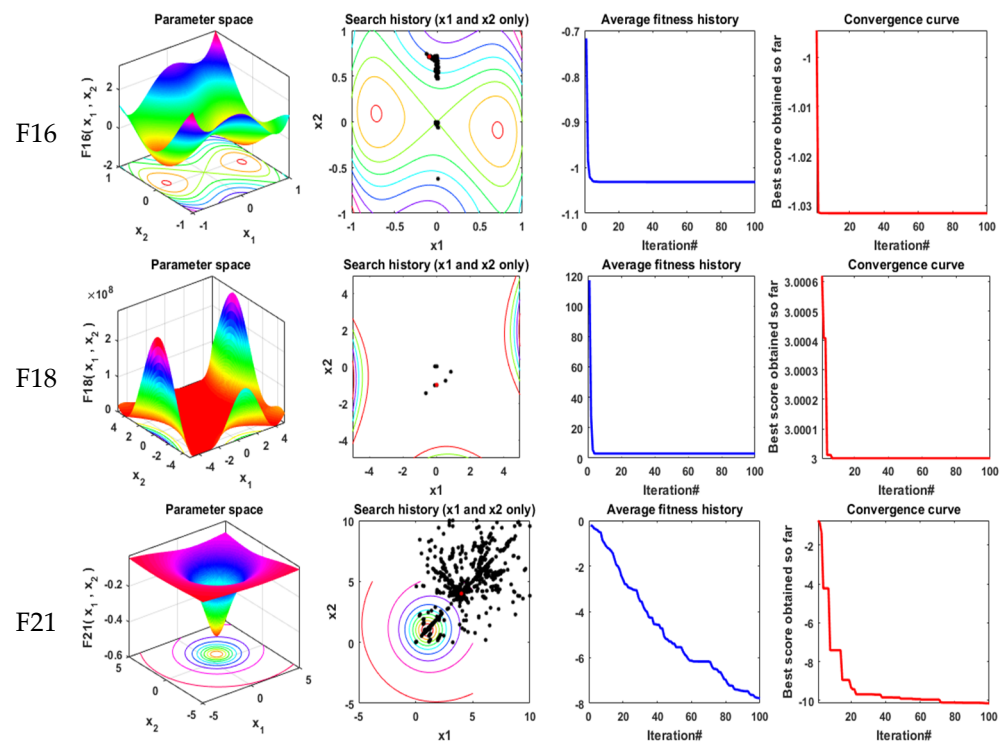


Figure 11. Qualitative metrics of nine benchmark functions: 2D views of the functions, search history, average fitness history, and convergence curve by the ESAOA technique.

Table 4. Statistical results of 23 benchmark functions using the ESAOA algorithm and other recent algorithms.

Function	ESAOA	AOA	GWO	TSA	SOA	
F1	Best	0.00	0.00	1.18×10^{-28}	1.94×10^{-18}	6.86×10^{-12}
	Mean	9.8×10^{-239}	8.8×10^{-285}	3.08×10^{-26}	1.3×10^{-16}	3.75×10^{-10}
	Median	0.00	0.00	5.62×10^{-27}	4.67×10^{-17}	7.39×10^{-11}
	Worst	2×10^{-237}	1.8×10^{-283}	2.44×10^{-25}	8.29×10^{-16}	4.92×10^{-9}
	Std.	0.00	0.00	5.74×10^{-26}	2.07×10^{-16}	1.08×10^{-9}
F2	Best	0.00	0.00	8.6×10^{-17}	1.3×10^{-11}	6.42×10^{-8}
	Mean	0.00	0.00	1.19×10^{-15}	1.58×10^{-10}	7.97×10^{-7}
	Median	0.00	0.00	4.02×10^{-16}	6.67×10^{-11}	3.26×10^{-7}
	Worst	0.00	0.00	5.3×10^{-15}	9.55×10^{-10}	4.55×10^{-6}
	Std.	0.00	0.00	1.51×10^{-15}	2.26×10^{-10}	1.1×10^{-6}
F3	Best	0.00	0.00	1.53×10^{-14}	1.62×10^{-13}	1.4×10^{-7}
	Mean	2.9×10^{-215}	2.7×10^{-263}	4.7×10^{-11}	8.02×10^{-11}	5.12×10^{-6}
	Median	0.00	0.00	9.86×10^{-12}	2.83×10^{-11}	3.04×10^{-6}
	Worst	5.9×10^{-214}	5.4×10^{-262}	2.78×10^{-10}	4.17×10^{-10}	3.01×10^{-5}
	Std.	0.00	0.00	8.6×10^{-11}	1.15×10^{-10}	6.97×10^{-6}
F4	Best	4.5×10^{-276}	0.00	8.52×10^{-10}	1.84×10^{-5}	2.71×10^{-5}
	Mean	1.73×10^{-8}	1.2×10^{-144}	7.77×10^{-9}	0.00012	0.000456
	Median	2.5×10^{-191}	2.8×10^{-225}	6.5×10^{-9}	7.34×10^{-5}	0.000165
	Worst	3.47×10^{-7}	2.3×10^{-143}	2.76×10^{-8}	0.000434	0.004392
	Std.	7.75×10^{-8}	5×10^{-144}	7.25×10^{-9}	0.000106	0.000975
F5	Best	5.322228	6.379585	6.048707	5.297881	6.588347
	Mean	6.615337	7.144313	6.603813	8.176168	7.671581
	Median	6.75582	7.101737	6.307698	8.726737	7.637013
	Worst	8.164718	7.970894	7.201725	8.980251	8.712294
	Std.	0.763634	0.387476	0.487729	1.111454	0.486548

Table 4. Cont.

Function		ESAOA	AOA	GWO	TSA	SOA
F6	Best	0.000294	0.009221	5.21×10^{-6}	0.256839	0.000565
	Mean	0.003079	0.037428	0.012663	1.019652	0.09884
	Median	0.002281	0.033666	1.46×10^{-5}	1.007907	0.026119
	Worst	0.010704	0.099548	0.252976	1.753997	0.251338
	Std.	0.002765	0.018338	0.056564	0.423224	0.116585
F7	Best	4.74×10^{-6}	9.81×10^{-6}	0.000163	0.00063	0.000224
	Mean	3.92×10^{-5}	8.59×10^{-5}	0.001104	0.004151	0.002663
	Median	3.99×10^{-5}	7.37×10^{-5}	0.000887	0.003798	0.002215
	Worst	8.69×10^{-5}	0.000286	0.003037	0.009982	0.00819
	Std.	2.23×10^{-5}	7.35×10^{-5}	0.000755	0.002746	0.001917
F8	Best	−4181.92	−2832.12	−3320.82	−3347.45	−2884.69
	Mean	−3989.31	−2578.88	−2628.94	−2622.61	−2368.36
	Median	−3997.67	−2644.75	−2558.71	−2612.42	−2302.53
	Worst	−3759.99	−2168.6	−2235.13	−2046.58	−2071.34
	Std.	114.5222	212.3066	311.404	368.3648	211.722
F9	Best	0.00	0.00	0.00	9.269193	3.62×10^{-10}
	Mean	0.00	0.00	2.045542	24.88918	2.566698
	Median	0.00	0.00	0.999332	26.08728	1.003987
	Worst	0.00	0.00	7.389995	40.12094	20.67609
	Std.	0.00	0.00	2.577417	9.094838	4.754352
F10	Best	8.88×10^{-16}	8.88×10^{-16}	6.48×10^{-14}	2.6×10^{-9}	3.8×10^{-7}
	Mean	8.88×10^{-16}	8.88×10^{-16}	1.37×10^{-13}	2.339824	6.978308
	Median	8.88×10^{-16}	8.88×10^{-16}	1.04×10^{-13}	3.187546	1.05×10^{-5}
	Worst	8.88×10^{-16}	8.88×10^{-16}	4.31×10^{-13}	3.610056	19.94676
	Std.	0.00	0.00	9.43×10^{-14}	1.552157	9.756868
F11	Best	0.00	0.00	0.00	0.203824	1.04×10^{-10}
	Mean	5.72×10^{-5}	2.22×10^{-9}	0.044072	0.530248	0.091855
	Median	0.00	0.00	0.018544	0.504302	0.068442
	Worst	0.001143	4.43×10^{-8}	0.159545	1.173223	0.307718
	Std.	0.000256	9.91×10^{-9}	0.047277	0.27678	0.090237
F12	Best	0.283422	0.723317	0.05936	3.537756	0.446997
	Mean	0.453052	0.785676	0.148302	12.19959	0.86591
	Median	0.459698	0.784702	0.141586	10.11875	0.869076
	Worst	0.538332	0.836673	0.394144	21.49549	1.511063
	Std.	0.060753	0.031815	0.075541	5.756827	0.301901
F13	Best	0.012385	0.657662	1.08×10^{-5}	0.323062	0.018692
	Mean	0.267522	0.833384	0.015311	0.763572	0.225589
	Median	0.257658	0.827932	2.82×10^{-5}	0.724039	0.204436
	Worst	0.715104	0.995477	0.102499	1.291658	0.426289
	Std.	0.165745	0.111759	0.037327	0.285704	0.116181
F14	Best	0.998004	1.992031	0.998004	0.998004	0.998004
	Mean	4.67887	9.38367	3.403167	8.206384	3.156667
	Median	2.982105	12.1946	1.990054	8.346013	0.998397
	Worst	12.67051	12.67051	10.76318	16.44091	10.76318
	Std.	3.698003	4.29236	3.464742	5.322547	3.450941
F15	Best	0.000307	0.000371	0.00031	0.000311	0.000446
	Mean	0.000854	0.00841	0.004464	0.007549	0.001148
	Median	0.000659	0.005623	0.000485	0.000528	0.00124
	Worst	0.004937	0.027434	0.020363	0.020944	0.00128
	Std.	0.001031	0.00893	0.008158	0.009779	0.000246

Table 4. Cont.

Function		ESAOA	AOA	GWO	TSA	SOA
F16	Best	−1.03163	−1.03163	−1.03163	−1.03163	−1.03163
	Mean	−1.03163	−1.03163	−1.03163	−1.03163	−1.03162
	Median	−1.03163	−1.03163	−1.03163	−1.03163	−1.03162
	Worst	−1.03163	−1.03163	−1.03163	−1.03163	−1.03161
	Std.	1.61 × 10^{−15}	1.6 × 10 ^{−7}	7.26 × 10 ^{−8}	4.32 × 10 ^{−7}	4.92 × 10 ^{−6}
F17	Best	0.397887	0.398228	0.397888	0.397892	0.397936
	Mean	0.397887	0.410557	0.3979	0.397983	0.398813
	Median	0.397887	0.410553	0.397891	0.397939	0.398382
	Worst	0.397889	0.427888	0.397936	0.398367	0.401669
	Std.	3.67 × 10^{−7}	0.00795	1.52 × 10 ^{−5}	0.000114	0.00108
F18	Best	3.00	3.00	3.00	3.000007	3.00
	Mean	3.00	8.400001	3.000097	4.35031	3.000158
	Median	3.00	3.00	3.000068	3.000054	3.000048
	Worst	3.00	30.00001	3.000436	30.00052	3.00182
	Std.	1.41 × 10^{−12}	11.08057	0.000109	6.037432	0.000399
F19	Best	−3.86278	−3.86032	−3.86278	−3.86275	−3.86275
	Mean	−3.86278	−3.84945	−3.86138	−3.86219	−3.85799
	Median	−3.86278	−3.84956	−3.86266	−3.86255	−3.85687
	Worst	−3.86278	−3.84003	−3.85516	−3.85634	−3.85396
	Std.	1.79 × 10^{−7}	0.005712	0.002624	0.001401	0.003535
F20	Best	−3.32198	−3.15504	−3.32198	−3.32041	−3.31737
	Mean	−3.26036	−3.04044	−3.23578	−3.23861	−3.08949
	Median	−3.31223	−3.08389	−3.20253	−3.26007	−3.07859
	Worst	−3.14596	−2.80747	−3.11704	−3.08284	−3.01103
	Std.	0.067456	0.101308	0.076637	0.08915	0.08515
F21	Best	−10.153	−8.4516	−10.1516	−9.97389	−10.0281
	Mean	−8.92258	−4.35691	−8.54697	−5.27743	−5.21172
	Median	−10.0688	−4.03416	−10.1433	−3.82522	−5.04103
	Worst	−2.63047	−1.88282	−2.62947	−2.60926	−0.49652
	Std.	2.435179	1.670435	2.896804	3.197572	4.05175
F22	Best	−10.4026	−5.68682	−10.4023	−10.3371	−10.117
	Mean	−9.9074	−3.61051	−10.3968	−7.59042	−7.34162
	Median	−10.3895	−3.50315	−10.3984	−9.89437	−9.74572
	Worst	−2.76541	−1.7743	−10.39	−1.82942	−0.90793
	Std.	1.699087	1.060224	0.003778	3.136193	3.369475
F23	Best	−10.5363	−8.47982	−10.5338	−10.4705	−10.3301
	Mean	−10.3325	−3.17706	−10.261	−5.73098	−6.45634
	Median	−10.4996	−3.05482	−10.5299	−3.73946	−7.39508
	Worst	−7.90191	−1.58983	−5.16879	−1.67163	−0.94612
	Std.	0.582497	1.628802	1.198578	3.891709	3.738585

The optimal values obtained are in bold.

Table 4 displays the statistical results of the proposed ESAOA technique and other recent techniques used for the 23 benchmark functions, such as the unimodal benchmark functions, multimodal benchmark functions, and composite benchmark functions. The optimal values acquired with the ESAOA algorithm, original AOA, GWO, TSA, and SOA algorithms are presented in bold. It can be seen that the ESAOA algorithm reaches the optimal result for most of these benchmark functions. From this table, it is found that the proposed strategy outperforms the other investigated algorithms and can be used as a new alternative tool for solving the nonlinear optimization problems. The convergence curve of each technique is another key part that should be studied for comparison purposes. The convergence curves of all algorithms for these benchmark functions are illustrated in Figure 12. It can be seen that the proposed ESAOA technique converges to a high-qualified solution with a faster rate than the conventional AOA and other algorithms. This proves

the superiority of the ESAOA not only in gaining accurate results but also in terms of the convergence rate to the optimal solutions. Moreover, the best boxplots for these algorithmic functions are presented in Figure 13. From these figures, it is clear that the proposed ESAOA technique achieved a stable point for all functions and the boxplots of the ESAOA algorithm are very narrow for many functions compared to the other algorithms.

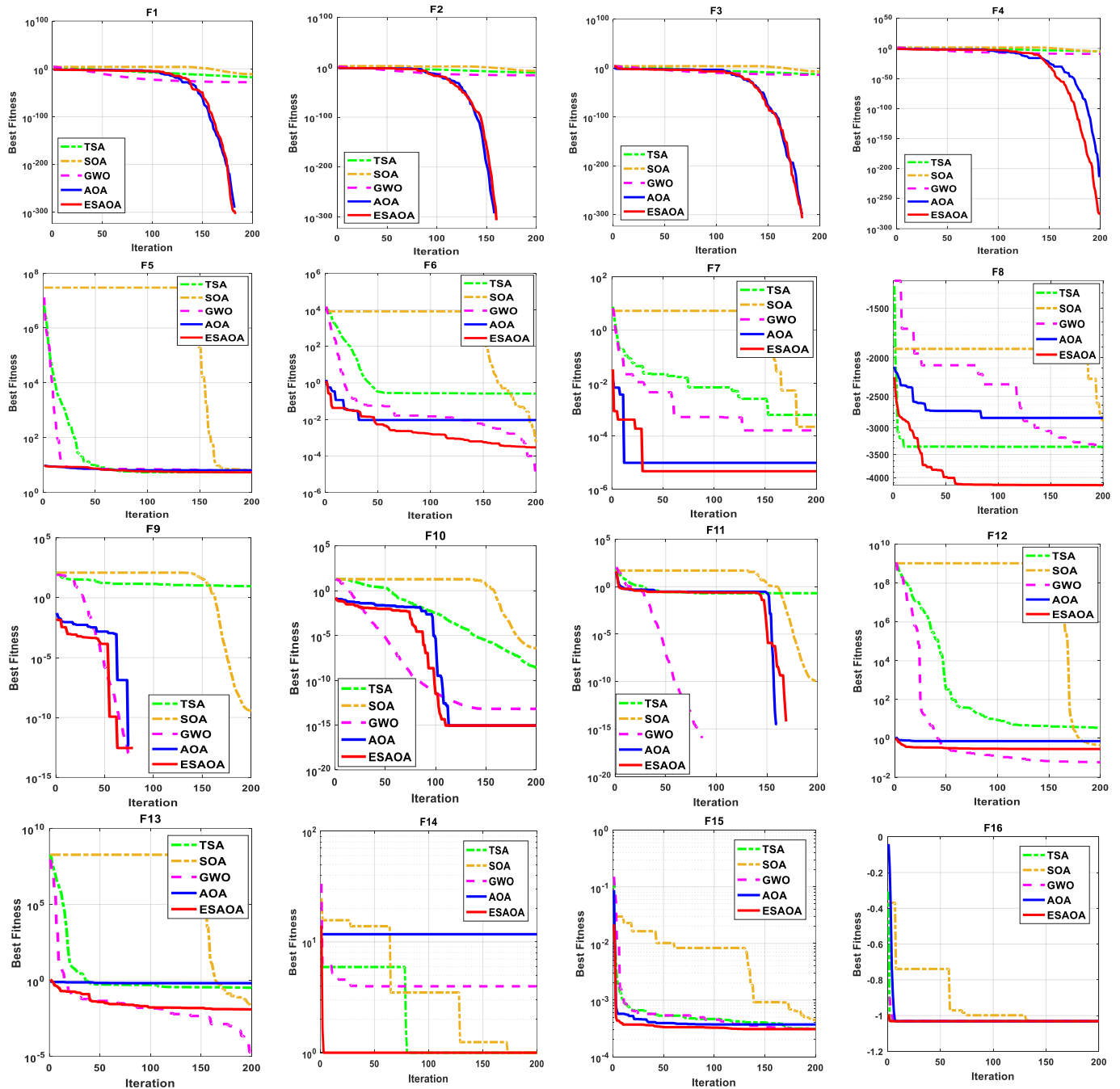


Figure 12. Cont.

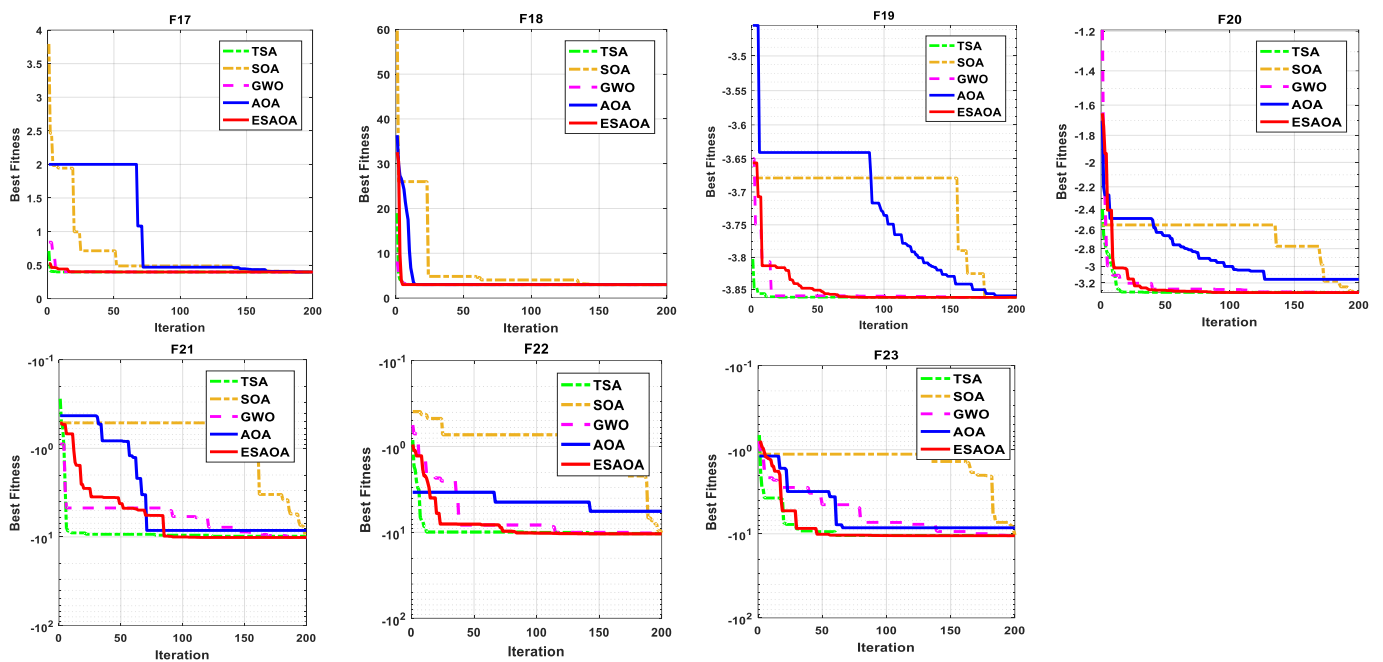


Figure 12. The convergence curves of all algorithms for 22 benchmark functions.

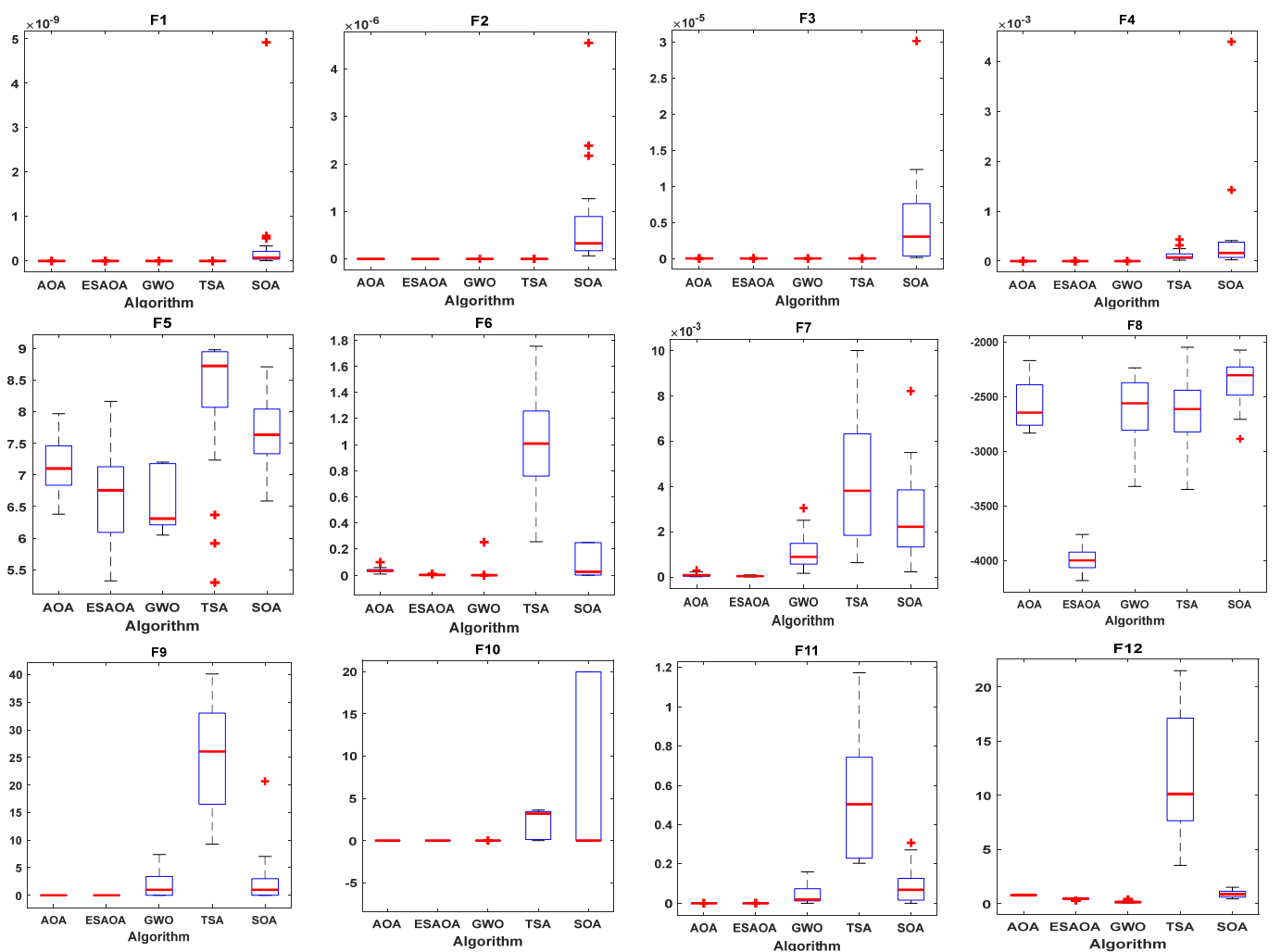


Figure 13. Cont.

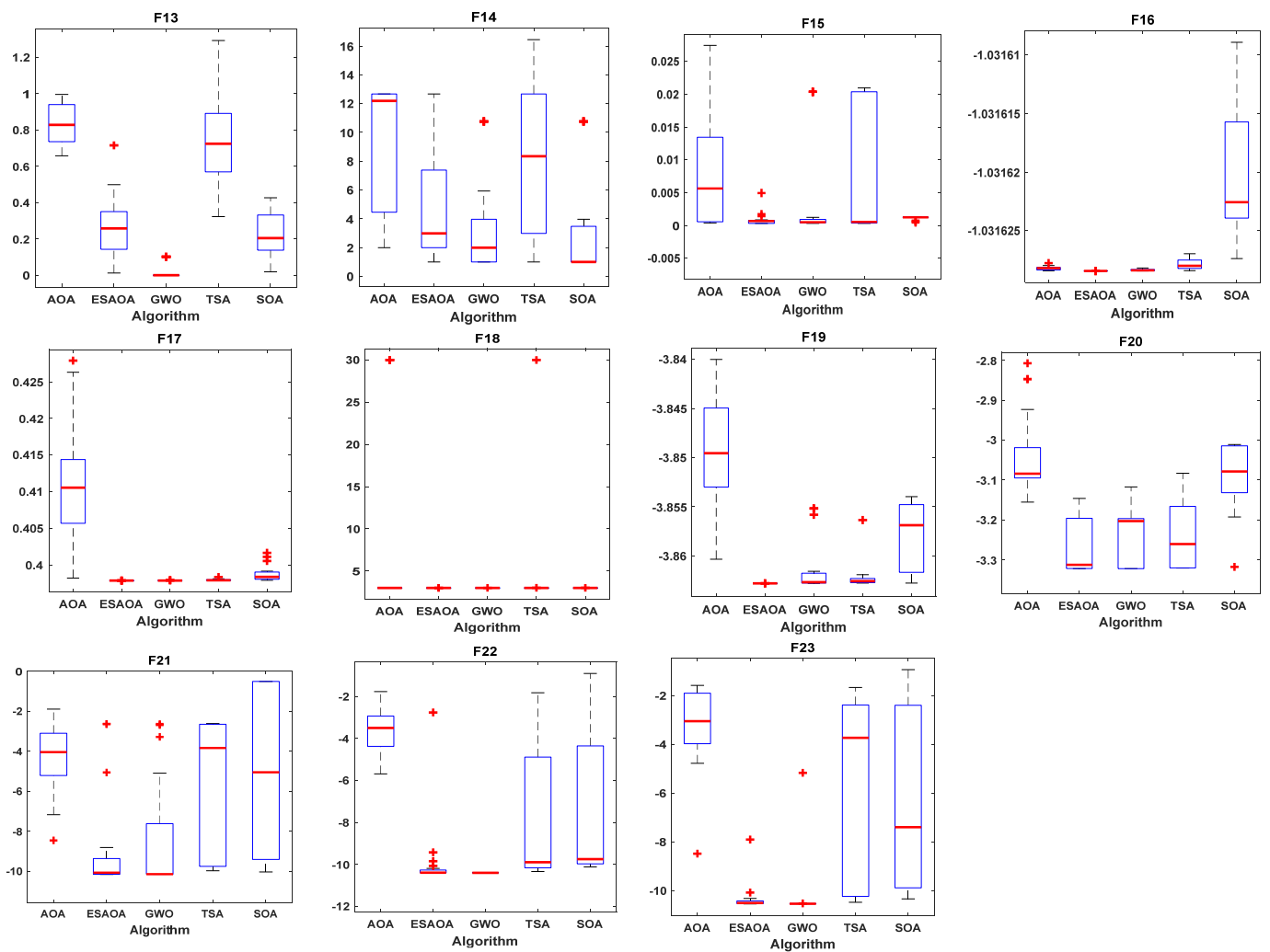


Figure 13. Boxplots for all algorithms for 23 benchmark functions.

The complexity of an algorithm is an important metric to judge its performance. The population initialization process of proposed ESAOA and other competitor algorithms (i.e., AOA, GWO, TSA, and SOA) requires $O(n_o \times n_p)$ time, where n_o and n_p represents the number of objectives and the number of population size, respectively. The complexity of calculating the fitness of search agents for all algorithms needs $O(Max_iter \times OF)$ where OF represents the objective function for a given problem. To simulate the whole procedure, it requires $O(N)$ time.

The computational complexity of the proposed ESAOA algorithm is $O(N \times Max_iter \times n_o \times n_p \times OF \times ES)$ where $O(ES)$ is the time for the eagle strategy. The computational complexities corresponding to AOA, SOA, and GWO algorithms are $O(N \times Max_iter \times n_o \times n_p \times OF)$. Whereas, the space complexity of all algorithms is the maximum amount of utilized space at any one time, which is considered during its initialization process.

Table 5 shows the values of the average CPU time of different algorithms on the 23 benchmark functions. It can be seen that the SOA and TSA algorithms take less time than other algorithms in terms of seconds, however they give the worst values for a majority of the 23 benchmark functions. Conversely, although the ESAOA algorithm takes a long time, it achieves the optimal solution for a majority of the 23 benchmark functions. These prove that the eagle strategy helps the proposed algorithm to avoid the local optima and improves its convergence characteristics.

Table 5. CPU time (s) of five techniques on 23 benchmark functions.

	ESAOA	AOA	GWO	TSA	SOA
F1	0.158067	0.157532	0.07462	0.073748	0.065735
F2	0.186421	0.122095	0.08423	0.084203	0.082134
F3	0.343078	0.305373	0.156705	0.160667	0.15203
F4	0.167088	0.119571	0.074367	0.079587	0.06675
F5	0.185138	0.144944	0.090093	0.087103	0.078565
F6	0.153903	0.161057	0.074578	0.073524	0.069944
F7	0.192688	0.185702	0.099875	0.105351	0.089709
F8	0.23918	0.195866	0.126665	0.101552	0.087846
F9	0.168967	0.110754	0.081035	0.07882	0.074222
F10	0.18238	0.189347	0.091267	0.089225	0.083114
F11	0.204376	0.134377	0.09552	0.097491	0.090226
F12	0.773338	0.474345	0.425797	0.414251	0.408157
F13	0.431127	0.25316	0.179413	0.182965	0.168955
F14	1.206234	0.648448	0.57518	0.565457	0.561881
F15	0.159681	0.119146	0.068502	0.076323	0.065716
F16	0.138274	0.096629	0.052976	0.05419	0.047642
F17	0.126026	0.111425	0.048627	0.049217	0.043522
F18	0.121769	0.107396	0.051741	0.048695	0.043093
F19	0.215938	0.143621	0.092925	0.098205	0.087989
F20	0.222126	0.171442	0.107665	0.102443	0.094654
F21	0.345999	0.446825	0.159064	0.159221	0.152833
F22	0.424687	0.25517	0.197564	0.19875	0.191696
F23	0.536892	0.324483	0.253615	0.254812	0.250334

4. Simulation Results

The model of the studied power grid has been built using MATLAB/SIMULINK[®] software (R2019b). Here, the studied model of the power grid consists of two-area interconnected power plants. Furthermore, the code of the proposed ESAOA method has been built using an M-file to perform the processes of selecting the optimal parameters of the PID and FOPID controllers. Furthermore, the simulation results are performed on hp type PC with Intel Core i5-2.60 GHz with 4.00 GB of RAM that manufactured in China. Various scenarios are methodically described in this research to estimate the studied system performance, which is summarized as follows:

- Scenario A: Estimation of system performance considering various types of load perturbations (i.e., step load perturbation (SLP), series SLP, and random load).
- Scenario B: Estimation of system performance considering high renewables penetration.
- Scenario C: Estimation of system performance considering RESs, a communication time delay of the studied control system.

Accordingly, the evaluation of the studied system performance is measured through the best objective function value over iterations. The *ITAE* represents the expression that indicates the objective function value to detect the strength of the system's performance. There are initial values that are taken into consideration while optimizing the proposed PID controller utilizing AOA and ESAOA as the number of search agents equaling 40 and the number of attempts/iterations equaling 100. Furthermore, there are proposed conditions that have been taken into consideration to have the convergence curve as the presented power system is a two-area interconnected power plant (each grid included by thermal, hydro, and gas) considering a 1% SLP at the first area only without any RESs penetration. Figure 14 shows the resulting convergence curve, which demonstrates the difference in performance between ESAOA and AOA. It also clarifies the strength of the ESAOA technique in reducing power system oscillations and attaining good performance compared to AOA utilizing the PID controller. The behavior of ESAOA from the convergence curve starts from an objective function near a value of 0.029 at the first iteration then it drops along iterations to end up at the final iteration to a value of 0.02 of the objective function.

The AOA behavior is summarized as beginning with a value of objective function near 0.029 and also drops along with attempts until reaches a value near 0.023.

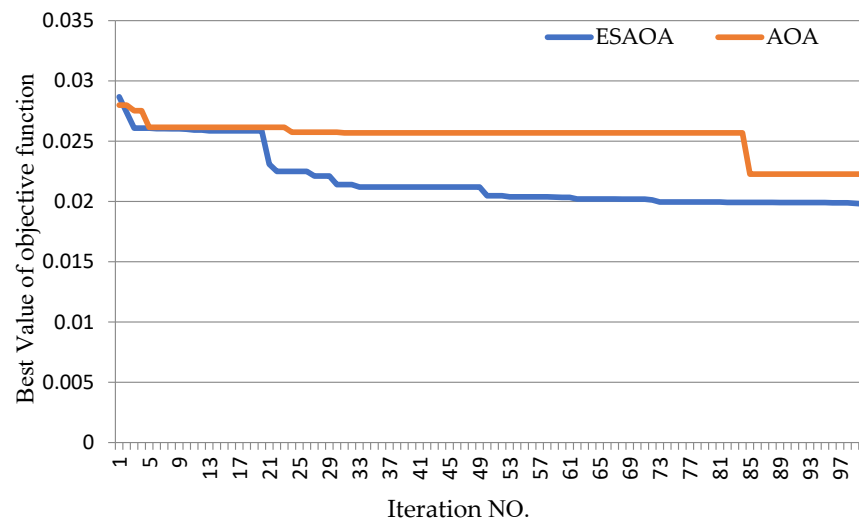


Figure 14. The convergence curve of the proposed PID controller using AOA and ESAOA techniques.

4.1. Scenario A: Estimation of System Performance under Various Types of Load Perturbation

This scenario presents a fair comparison between the proposed FOPID controller-based ESAOA and other previous works utilizing PID-based TLBO, AOA, and ESAOA in stabilizing the power system frequency. The proposed ESAOA and other applied techniques (i.e., TLBO and AOA) efficiency have been tested by applying different load variation types (i.e., SLP, series SLP, and random load disturbance).

Case A.1: This section explicates the different dynamic studied system responses (i.e., Δf_1 , Δf_2 , and Δp_{tie}) while applying a 1% SLP in the first area of the two-area interconnected power grid. The applicable load perturbation is at the tenth second ($t = 10$ s) of the simulation time to check the robustness of the proposed ESAOA in obtaining the optimum parameters that achieve more system stability. The utilized SLP represents residential loads that are connected suddenly to the grid. This type of load variation may be represented by the disconnection of some generators from the total generation station that may lead to a shutdown of all stations' generators. In addition, SLP may be represented as an unexpected switch of the connected electrical loads that may lead to instability in the system performance by increasing wear and tear on generators. Table 6 indicates the optimal PID controller parameters utilizing ESAOA and AOA algorithms, optimal FOPID controller parameters based on ESAOA, as well as the parameters of the PID controller based on TLBO. Figure 15 clears the system performance of this case. Note that the proposed ESAOA, which applied to obtain the FOPID controller parameters, achieves more system stability compared to other mentioned techniques.

Table 6. The optimal controllers' values for scenario A.1.

Controller Properties	Thermal	Hydro	Gas
PID relied on TLBO	$k_p = 4.1468, k_i = 4.0771, k_d = 2.0157$	$k_p = 1.0431, k_i = 0.6030, k_d = 2.2866$	$k_p = 4.7678, k_i = 3.7644, k_d = 4.9498$
PID relied on AOA	$k_p = 10, k_i = 1.5975, k_d = 2.7449$	$k_p = 1.5975, k_i = 0.0837, k_d = 0.0875$	$k_p = 10, k_i = 10, k_d = 1.2779$
PID relied on ESAOA	$k_p = 10, k_i = 1.4842, k_d = 6.1277$	$k_p = 9.6838, k_i = 0.0147, k_d = 0.3501$	$k_p = 1.4133, k_i = 9.8516, k_d = 0.1690$
FOPID relied on ESAOA	$k_p = 8.9645, k_i = 9.9979, k_d = 9.7397, \lambda = 0.7266, \mu = 0.8519$	$k_p = 6.6278, k_i = 9.1570, k_d = 4.631, \lambda = 0.587, \mu = 0.0887$	$k_p = 9.7594, k_i = 9.9997, k_d = 7.976, \lambda = 0.9159, \mu = 0.3775$

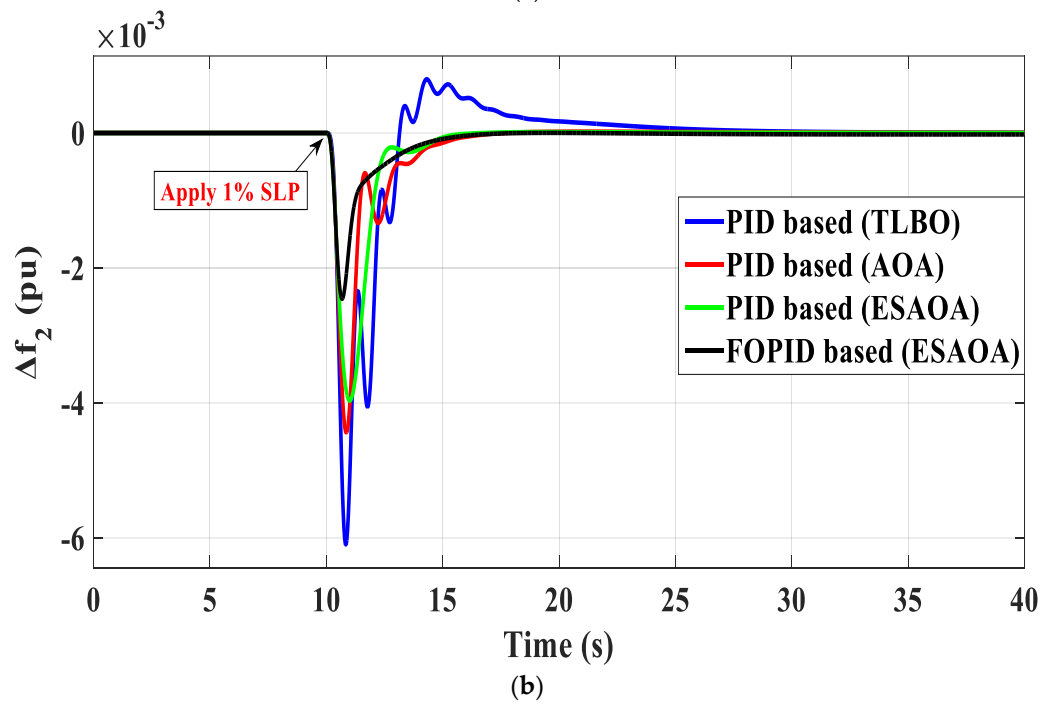
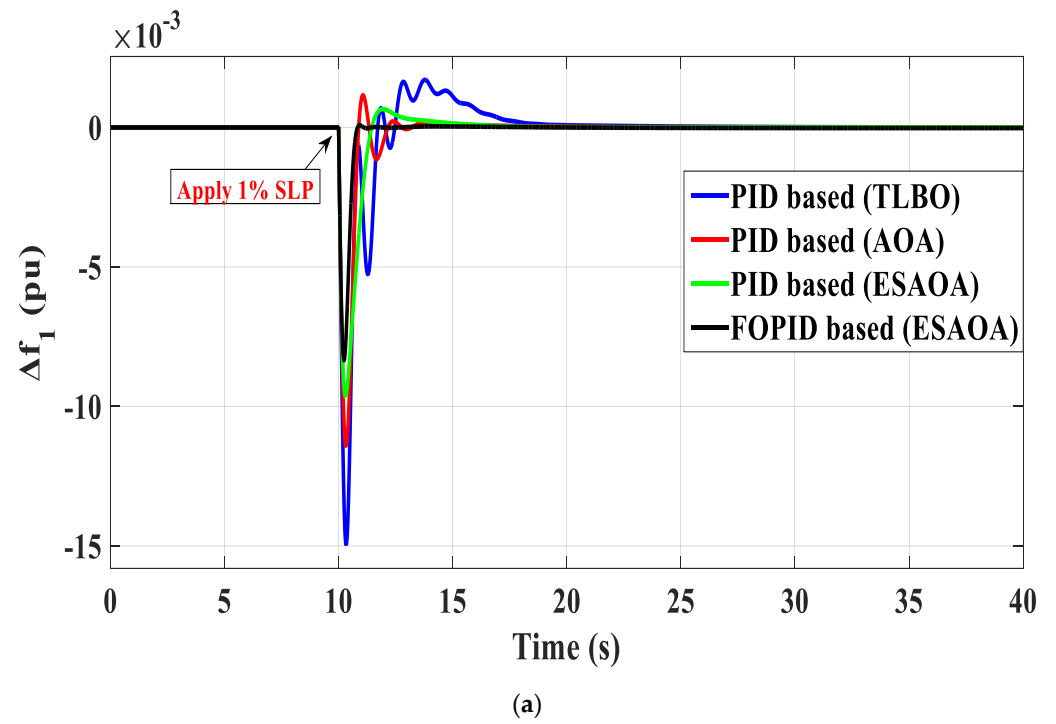


Figure 15. Cont.

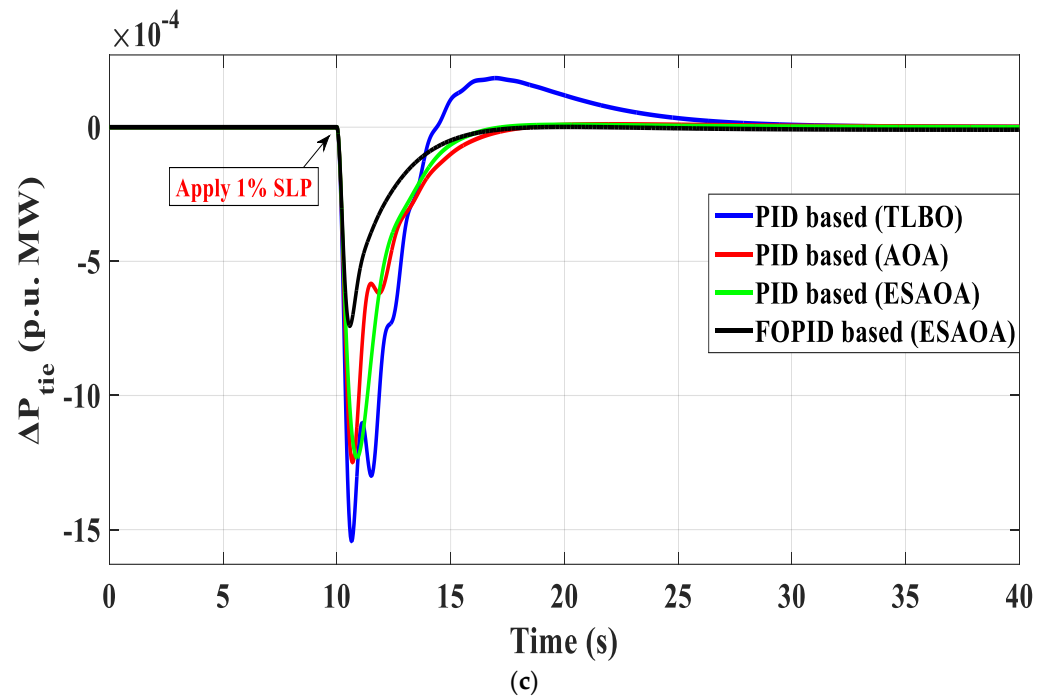


Figure 15. Dynamic system response of scenario A considering 1% SLP at the first area (a) Δf_1 , (b) Δf_2 , and (c) Δp_{tie} .

Table 7 presents the specifications of system performance, overshoot (OS), and undershoot (US) of the proposed FOPID controller using ESAOA and other mentioned controllers using different techniques (i.e., AOA and TLBO). It is noticeable that the FOPID controller-based ESAOA ensures better performance than the PID controller depending on TLBO, AOA, and ESAOA by gaining little OSs and USs values.

Table 7. Transient response specifications of the investigated system for scenario A.1.

Different Dynamic Responses	PID-Based TLBO	PID-Based AOA	PID-Based ESAOA	FOPID-Based ESAOA
	OS & US $\times (10^{-3})$			
Dynamic response of (Δf_1)	1.7217 −19.7259	1.158 −11.42	0.9417 −9.7290	0.0802 −8.344
Dynamic response of (Δf_2)	0.4363 −12.7986	0.02096 −4.443	0.01903 −3.8716	0.0018 −2.456
Dynamic response of (Δp_{tie})	0.1712 −3.0782	0.01107 −1.249	0.010812 −1.1782	0.001096 −0.74032

Case A.2: This case shows the dynamic system performance according to applying series SLP at the first area of the investigated power system to ensure the effectiveness of the proposed controller with the proposed optimization method in obtaining more system stability. The series SLP type is implemented to the investigated power system to emulate the realistic load variation. It also represents the series forced switch of generators or series interrupt of the connected loads. This type of load variation is formed in Figure 16. All dynamic system responses are shown in Figure 17. Figure 17 illustrates that the proposed ESAOA still can overcome the oscillations caused by series SLP.

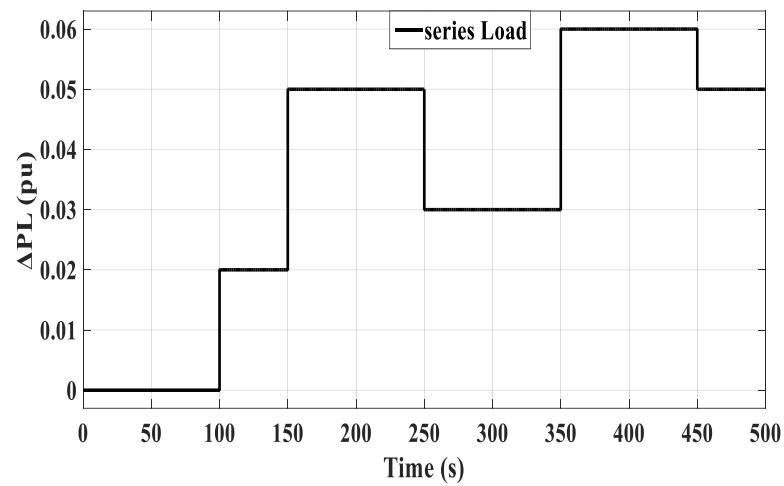


Figure 16. The form of the applied series SLP.

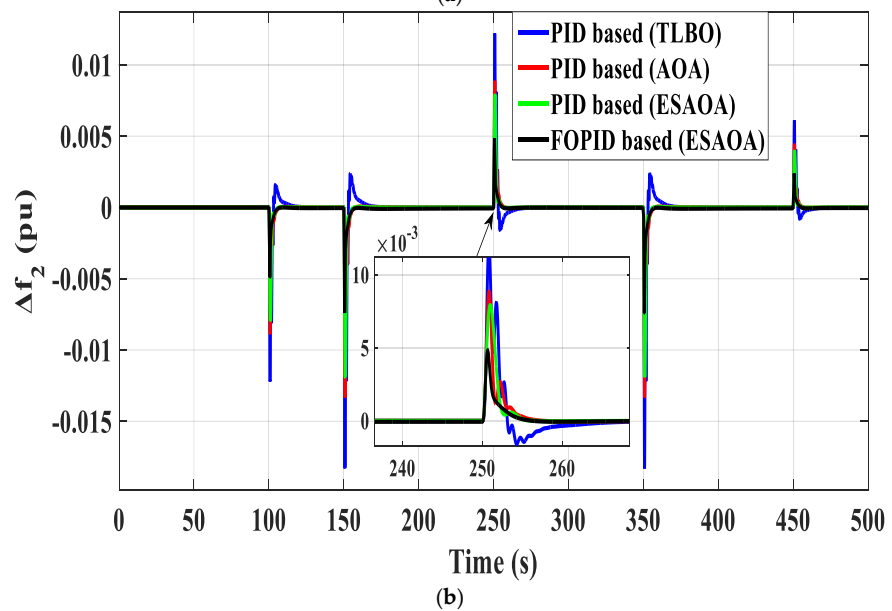
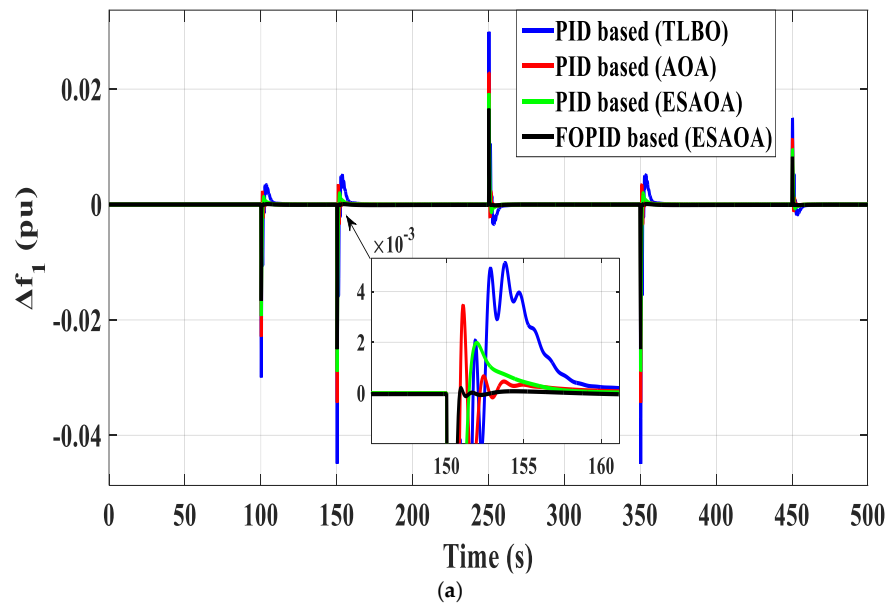


Figure 17. Cont.

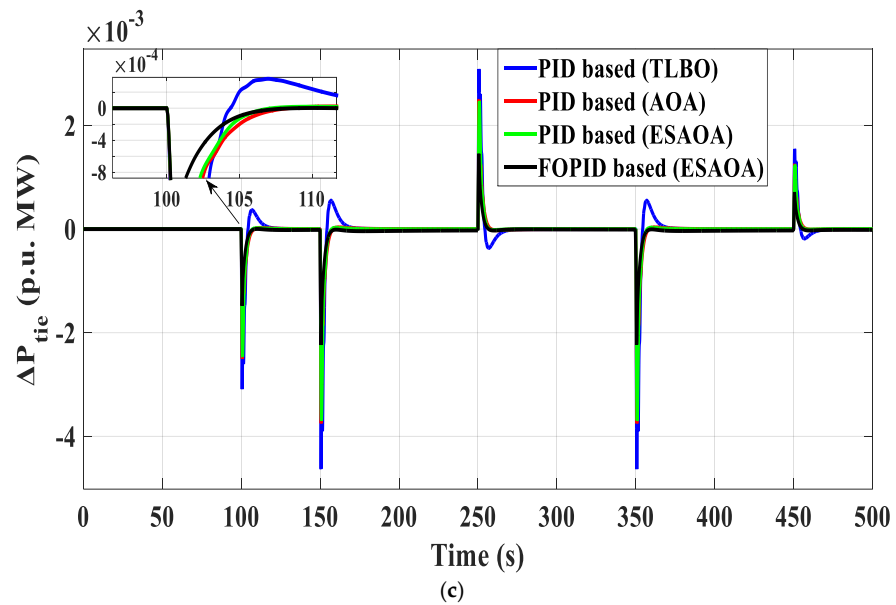


Figure 17. Dynamic system response of scenario A with series SLP at the first area (a) Δf_1 , (b) Δf_2 , and (c) Δp_{tie} .

Case A.3: The robustness of the proposed FOPID controller utilizing ESAOA considering random load variation in the first area is tested and illustrated in this section. The random load variance represents industrial loads that are connected to the grid serially. This random load is a combination of series SLP that can be represented by a series outage of generation units from the power station or series disconnection of electrical loads which lead to imbalance in the power system. The random load variation is formed in Figure 18. In addition, Figure 19 shows all dynamic power system responses, which explain the ability of the proposed FOPID controller in achieving system stabilization under this challenge.

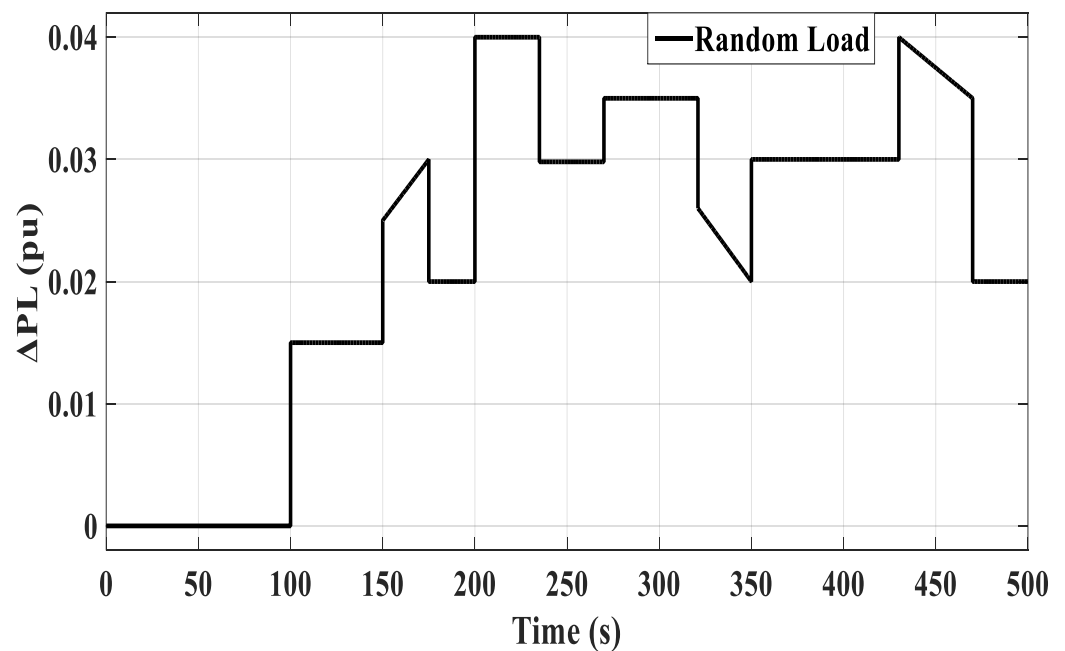
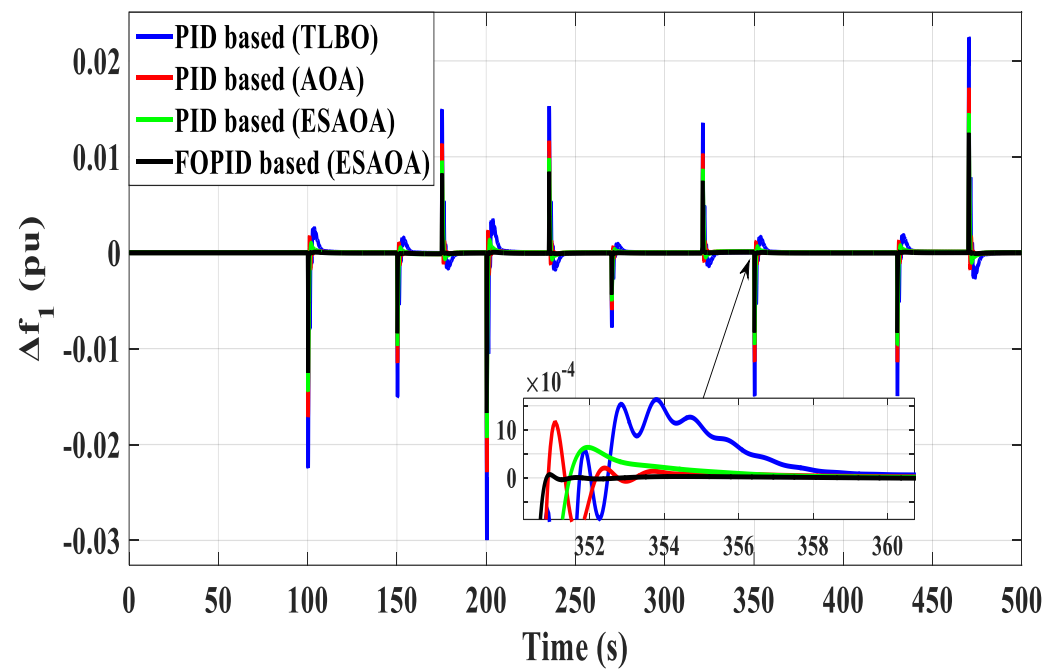
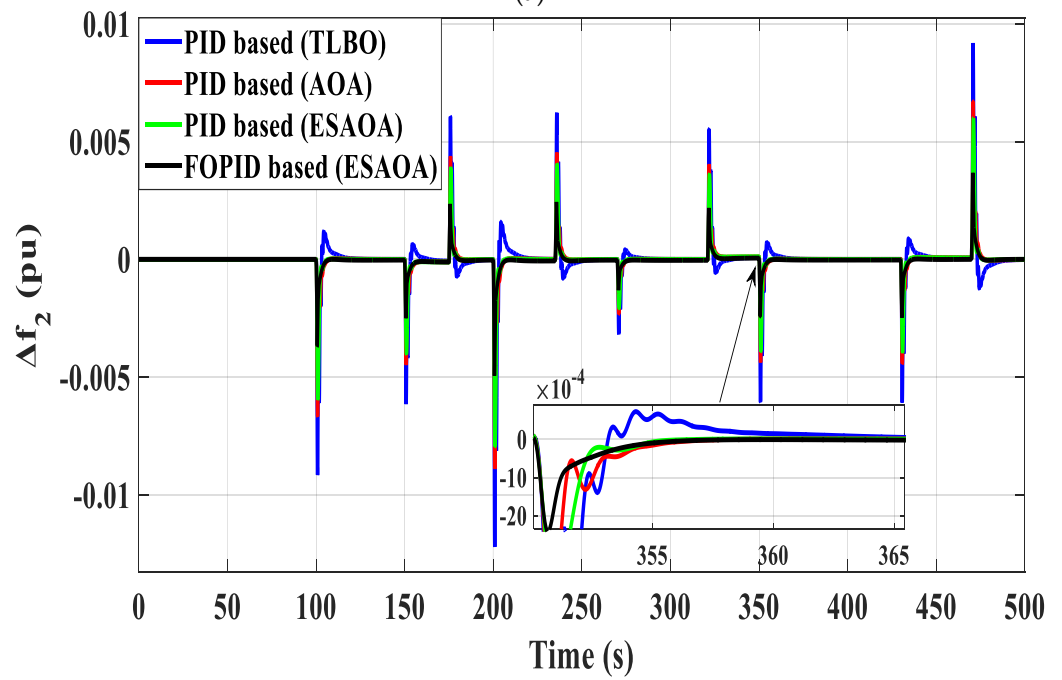


Figure 18. The form of applied random load variation.



(a)



(b)

Figure 19. Cont.

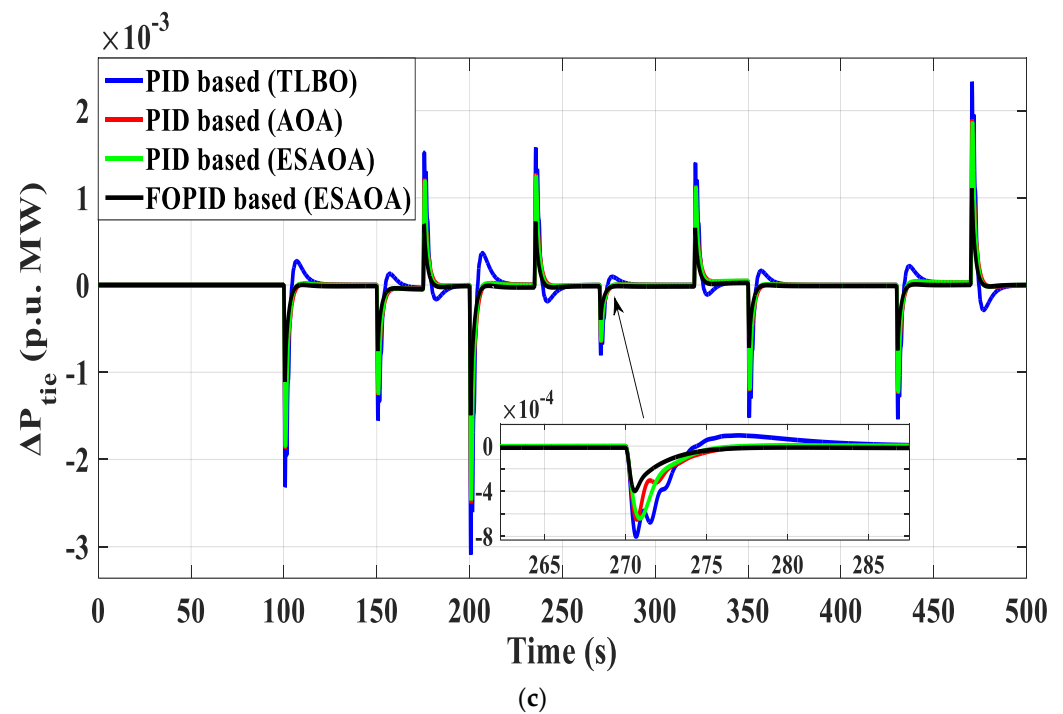


Figure 19. Dynamic system response of scenario A with random load variation at the first area (a) Δf_1 , (b) Δf_2 , and (c) Δp_{tie} .

4.2. Scenario B: Estimation of System Performance Considering RESs

This scenario presents another challenge by penetrating high RESs besides adding different load variations in the studied system. RESs are penetrated in both areas (i.e., wind energy in the first area and PV energy in the second area). Whereas, the penetration of RESs represents a burden on the studied system according to their drawbacks (i.e., lack of system inertia). The ESAOA is proposed to select the proposed PID and FOPID controllers considering high RESs penetration besides applying series SLP and random variation.

4.2.1. Case B.1: Robustness Test of Proposed PID Controller Using ESAOA Considering Series Step Load Variation

This section clarifies the dynamic system performance of the investigated power system taking into consideration a series SLP, high penetration of wind energy at $t = 450$ s at the first area, and PV at $t = 750$ s at the second area. Table 8 introduces the obtained optimal PID and FOPID controllers using the proposed ESAOA. The challenge of series SLP that shown previously in Figure 16 has been applied in the first area of the investigated system. In addition, all dynamic system responses represented in Δf_1 , Δf_2 , and Δp_{tie} are shown in Figure 20. The reliability of the proposed FOPID controller adjusted through ESAOA is assessed by testing it in damping the oscillations generated from series SLP and RESs. The proposed FOPID controller achieved an outstanding performance to gain stabilizing the system frequency and tie-line exchanged power.

Table 8. The optimal controllers' values for scenario B.

Controller Properties	Thermal	Hydro	Gas
PID relied on ESAOA	$k_p = 10, k_i = 10, k_d = 10$	$k_p = 10, k_i = 0.001, k_d = 2.9009$	$k_p = 10, k_i = 10, k_d = 4.5061$
FOPID relied on ESAOA	$k_p = 9.9899, k_i = 9.9254, k_d = 10, \lambda = 0.7864, \mu = 0.9910$	$k_p = 7.4207, k_i = 9.454, k_d = 6.4981, \lambda = 0.6064, \mu = 0.628$	$k_p = 0.7448, k_i = 9.9835, k_d = 9.9533, \lambda = 0.8786, \mu = 0.0227$

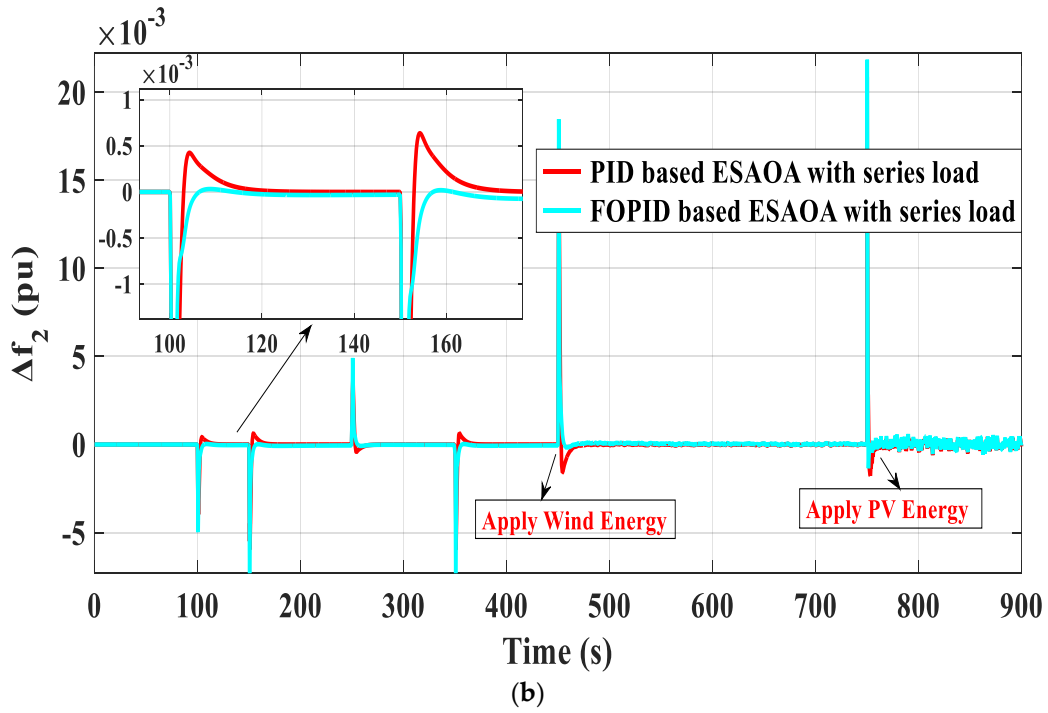
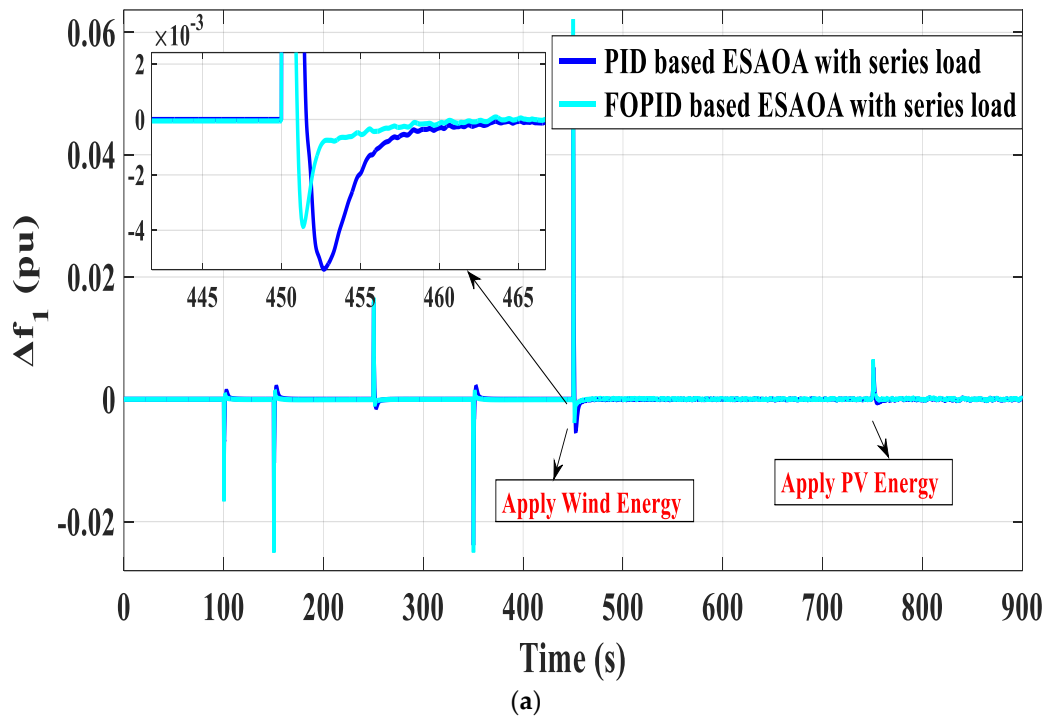


Figure 20. Cont.

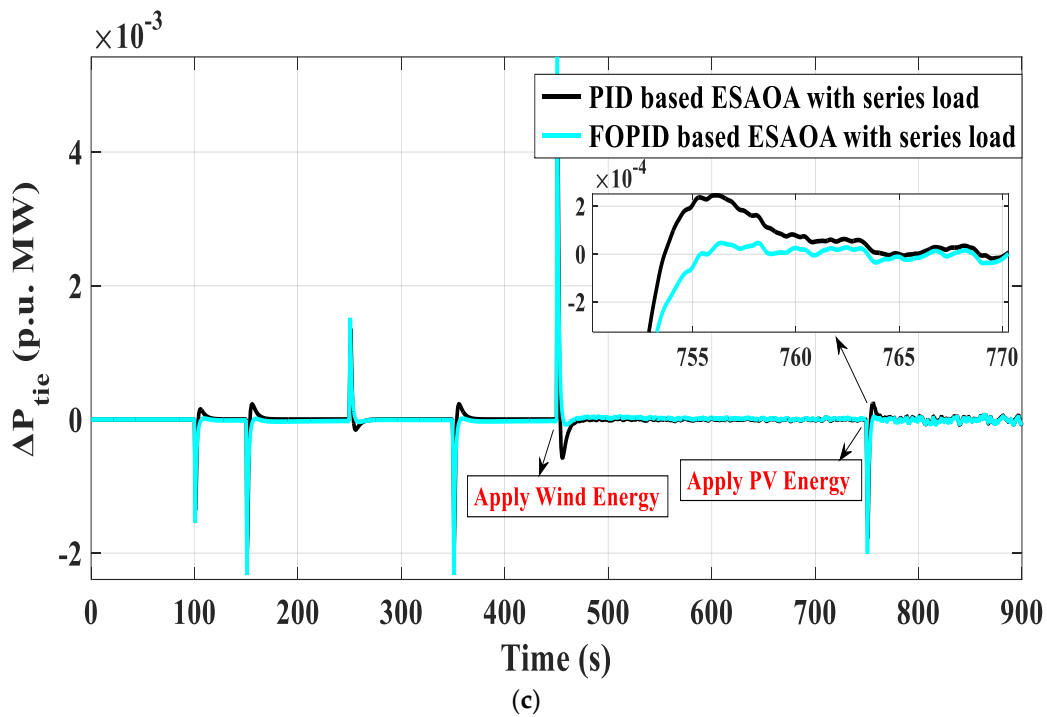


Figure 20. Dynamic system response of scenario B with series SLP at area-1, wind energy at $t = 450$ s at area-1, and PV at $t = 750$ s at area-2 (a) Δf_1 , (b) Δf_2 , and (c) Δp_{tie} .

4.2.2. Case B.2: Robustness Test of Proposed PID Controller Using ESAOA Considering Random Load Variation

A random load variation is applied in the first area of the studied power plant considering a high penetration of RESs at area-1 and area-2 to ensure that the obtaining of FOPID controller parameters using ESAOA can overcome the oscillations and stabilize the frequency of the studied system for achieving stability and security. The proposed random load perturbation that formed previously in Figure 18 has been applied in the first area of the studied model. The waveforms' behavior of frequency in both areas and the tie-line power are shown in Figure 21 with the challenge of RESs penetration and random load variation in the studied system. Good system performance is obtained through utilizing ESAOA in adjusting the FOPID controller to get optimal parameters that damp oscillations considering random load and penetrating RESs with a high-level percentage in the studied system.

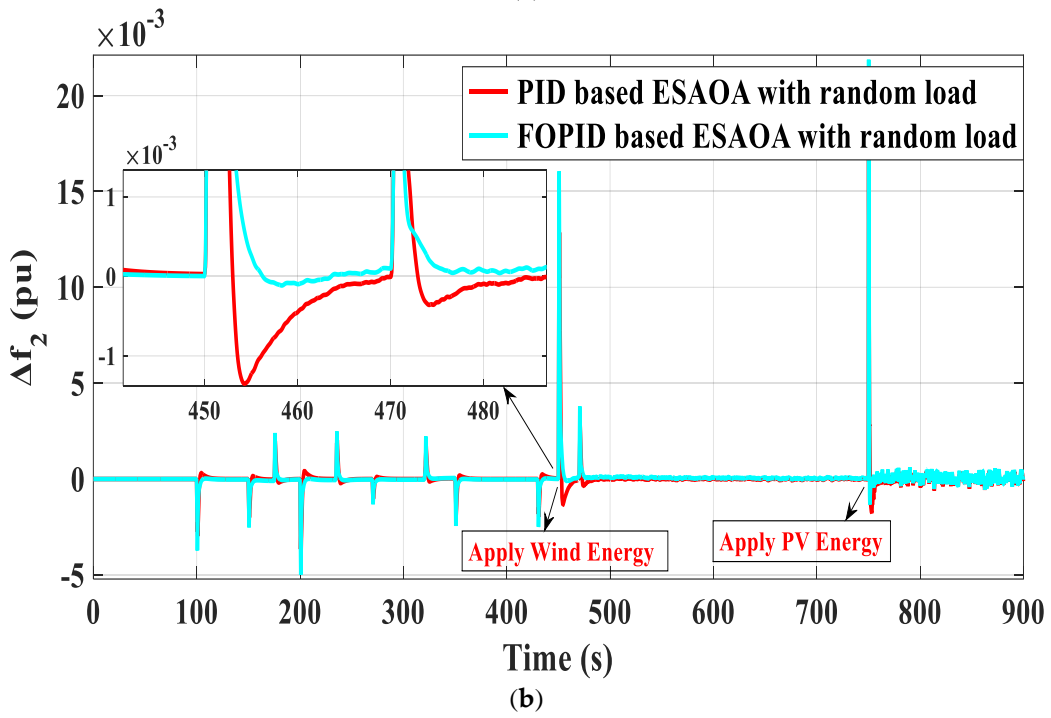
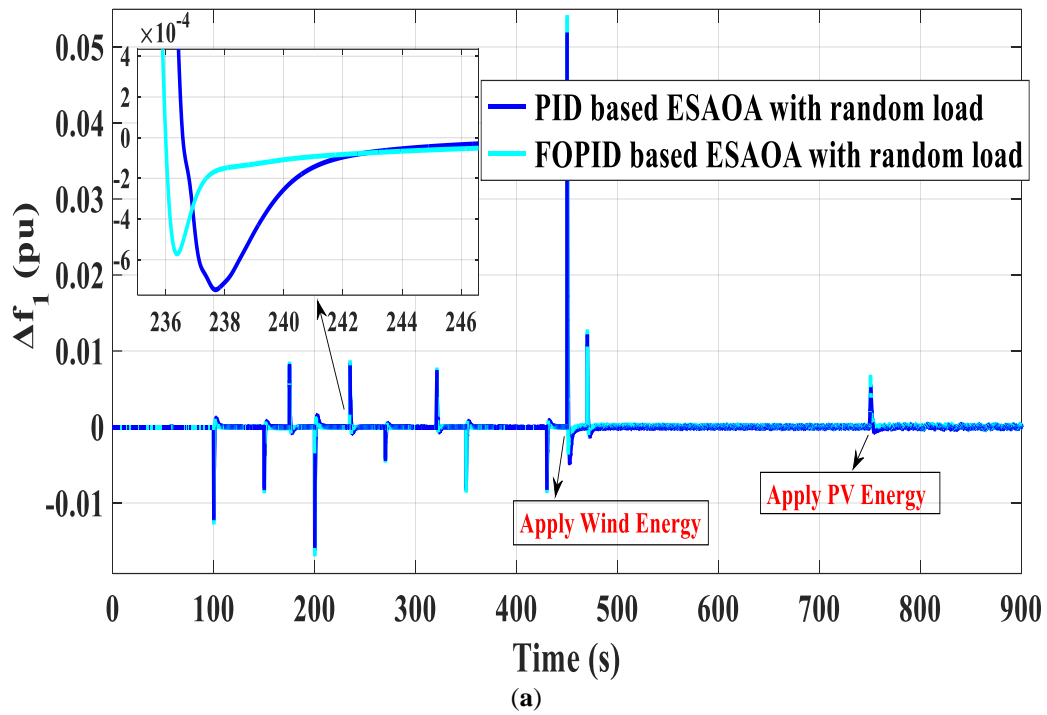


Figure 21. Cont.

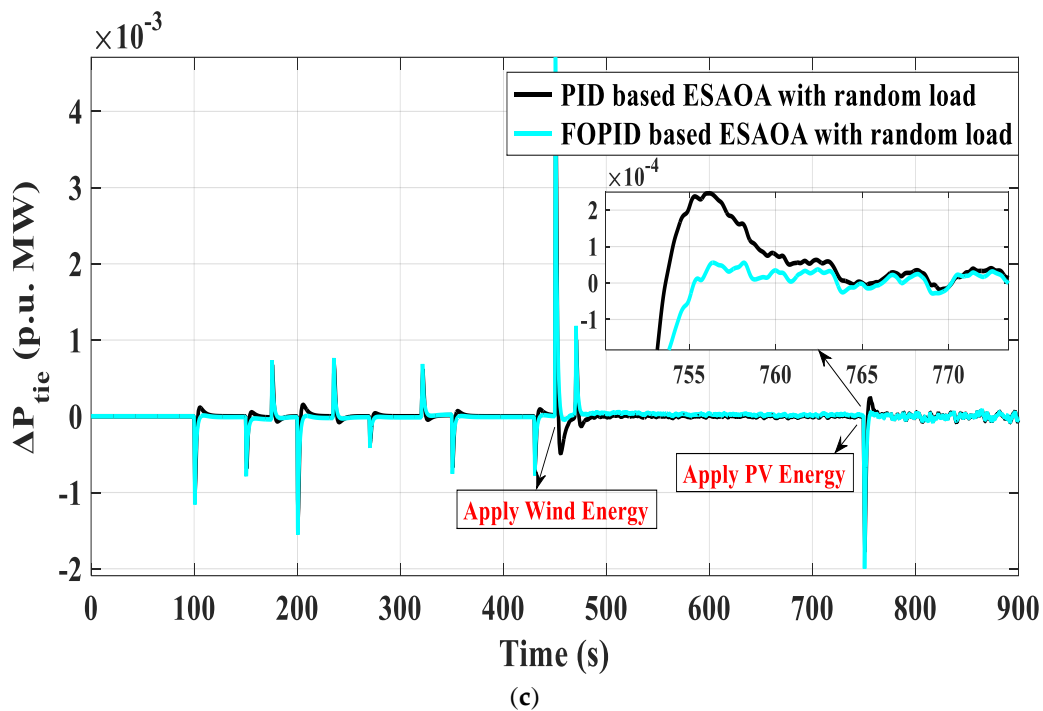


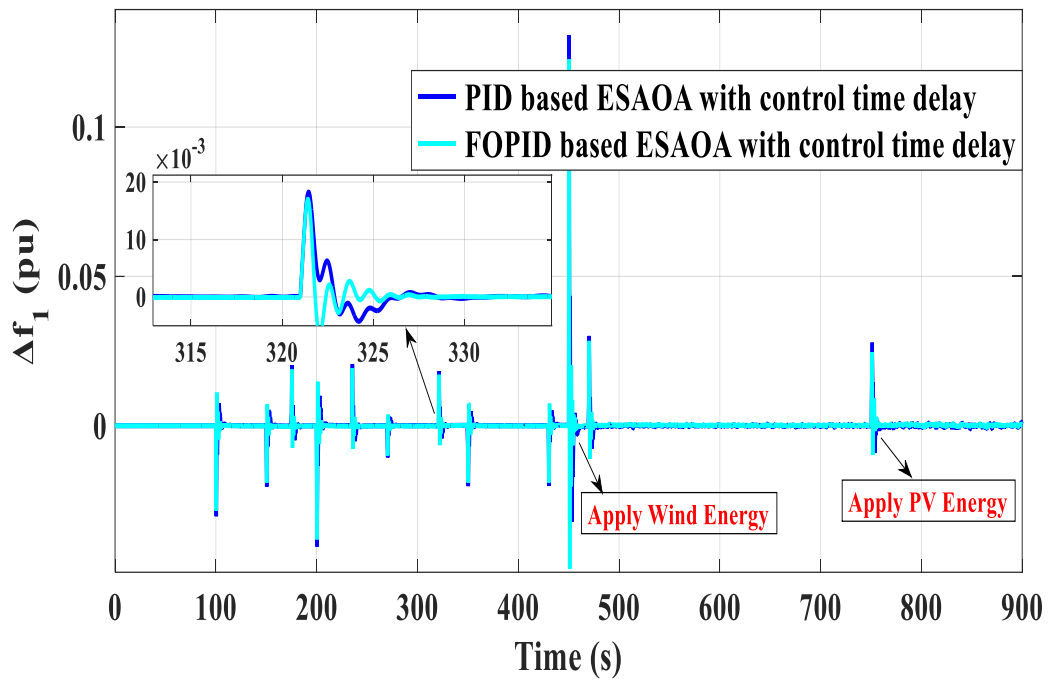
Figure 21. Dynamic system response of scenario B with random load variation at area-1, wind energy at $t = 450$ s at area-1, and PV at $t = 750$ s at area-2 (a) Δf_1 , (b) Δf_2 , and (c) Δp_{tie} .

4.3. Scenario C: Estimation of System Performance Considering RESs with Control System Time-Delay

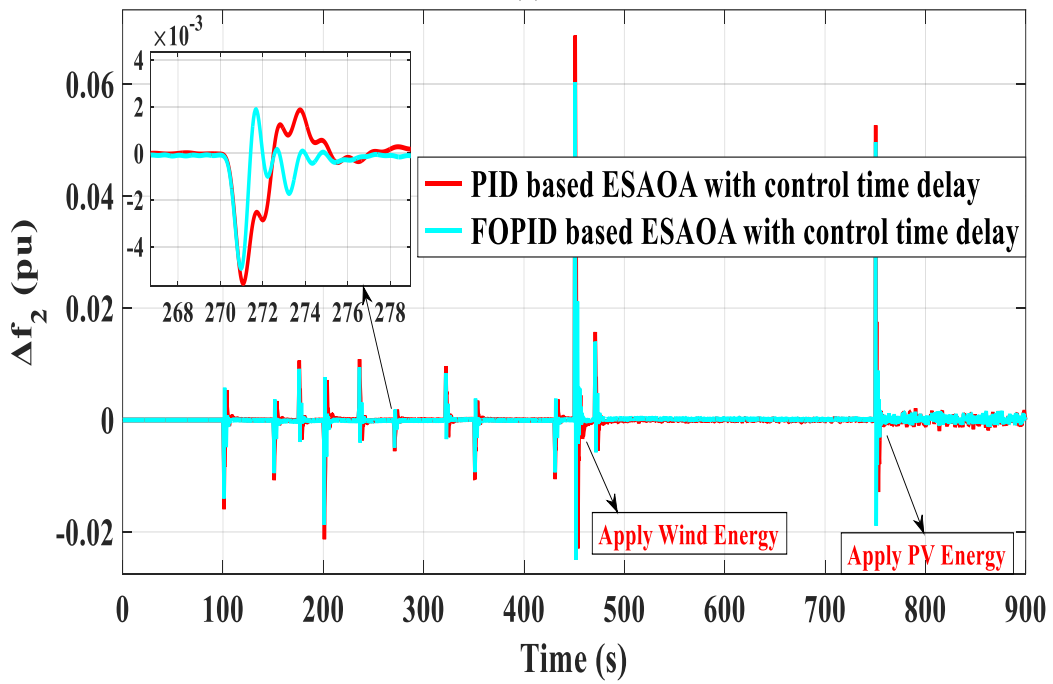
In this scenario, the communication control system time delay challenge is applied in the proposed studied system considering random load variation and penetration of RESs for ensuring the validity of the proposed modified technique based on a FOPID controller. The communication control system time delay is applied in the studied power system as a robust challenge on the proposed FOPID controller that is tuned by the proposed technique ESAOA to test its ability in enhancing the power system performance. The value of the time-delay, which is before and after the proposed FOPID controller action is 0.1 s. In addition, a random load variation is applied at area-1, wind energy is penetrated in area-1 at $t = 450$ s, and PV energy at area-2 at $t = 750$ s. Table 9 introduces the optimal obtained PID and FOPID controllers using the proposed ESAOA. The applied random load in the first area is formed previously in Figure 18. In addition, all dynamic system responses represented in Δf_1 , Δf_2 , and Δp_{tie} are shown in Figure 22. It can be seen from Figure 22 that the proposed ESAOA-based FOPID controller can still overcome the influence of random connected load variations, penetration of RESs, and communication time delay of the controller system. Therefore, the deviation in both area frequencies and tie-line power exchange has been regulated quickly to stabilize to zero (pre-defined value).

Table 9. The optimal controllers’ values for scenario C.

Controller Properties	Thermal	Hydro	Gas
PID relied on ESAOA	$k_p = 1.0463, k_i = 1.7939,$ $k_d = 4.4269$	$k_p = 3.7469, k_i = 0.8225,$ $k_d = 0.0246$	$k_p = 4.1489, k_i = 4.9518,$ $k_d = 0.5031$
FOPID relied on ESAOA	$k_p = 2.5448, k_i = 4.9311,$ $k_d = 5.980,$ $\lambda = 0.6686, \mu = 1$	$k_p = 7.6064, k_i = 9.7157,$ $k_d = 1.1185,$ $\lambda = 0.7057, \mu = 0.3877$	$k_p = 9.3985, k_i = 3.5022,$ $k_d = 2.3587,$ $\lambda = 0.3585, \mu = 0.4972$



(a)



(b)

Figure 22. Cont.

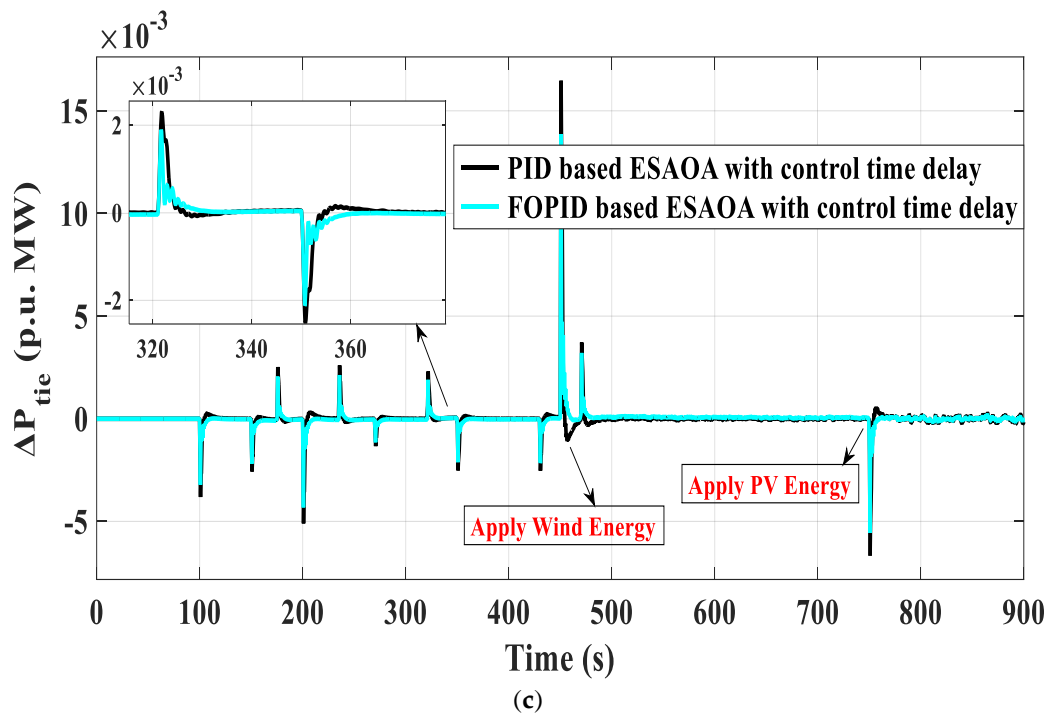


Figure 22. Dynamic system response of scenario C with random load variation at area-1, wind energy at $t = 450$ s at area-1, and PV at $t = 750$ s at area-2 considering communication time-delay (a) Δf_1 , (b) Δf_2 , and (c) Δp_{tie} .

5. Conclusions

This manuscript presents several main points as follows:

- Proposing the PID and FOPID controllers as a secondary controller to regulate the frequency of the studied power plant.
- A hybrid power grid consisting of three conventional power plants (i.e., thermal, hydro, and gas) is presented in this work to evaluate the efficacy of the proposed PID controller.
- Utilizing an improved algorithm labeled an eagle strategy arithmetic optimization algorithm (ESAOA) to select the optimum values of the proposed FOPID controller parameters according to good features of exploration and exploitation strategies of the proposed algorithm.
- A fair maiden comparison between the performance of the proposed algorithm ESAOA and other algorithms, such as TLBO and AOA, has been presented to ensure the robustness of the proposed technique in obtaining the optimal controller parameters.
- Proposing different scenarios to validate the robustness of the proposed FOPID controller that relies on ESAOA in overcoming the LFC problem in the studied system, such as applying several types of load variations (i.e., SLP, series SLP, and random load variation), penetrating of RESs with a high level, and applying the communication time delay before and after the proposed controller.
- The simulation results in this work ensure the robustness of the FOPID controller relied on ESAOA compared to the PID controller that relies on TLBO, AOA, and ESAOA in regulating the studied system frequency.

Furthermore, several efforts should be studied in the future work to test the effectiveness of the proposed PID controller considering flexible AC transmission systems (FACTS) devices, electrical vehicles (EVs), and increasing the studied areas (instead of a two-area, there will be a three-area and four-area interconnected power plant).

Author Contributions: Conceptualization, A.H.A.E., S.K., M.H.H., M.K. and E.M.A.; data curation, E.M.A.; formal analysis, A.H.A.E., M.K. and M.H.H.; funding acquisition, E.M.A. and S.K.; investigation, A.H.A.E., M.K. and M.H.H.; methodology, E.M.A. and S.K.; project administration, A.H.A.E., M.K. and M.H.H.; resources, E.M.A. and S.K.; supervision, S.K. and E.M.A.; validation, A.H.A.E., M.K. and M.H.H.; visualization, A.H.A.E., M.K. and M.H.H.; writing-original draft, A.H.A.E., M.K. and M.H.H.; writing-review and editing, E.M.A. and S.K. All authors have read and agreed to the published version of the manuscript.

Funding: This work was funded by the Deanship of Scientific Research at Jouf University under grant No (DSR-2021-02-0305).

Institutional Review Board Statement: Not applicable.

Informed Consent Statement: Not applicable.

Data Availability Statement: Not applicable.

Conflicts of Interest: The authors declare no conflict of interest.

References

1. Khamies, M.; Magdy, G.; Selim, A.; Kamel, S. An improved Rao algorithm for frequency stability enhancement of nonlinear power system interconnected by AC/DC links with high renewables penetration. *Neural Comput. Appl.* **2021**, *34*, 2883–2911. [[CrossRef](#)]
2. Setiadi, H.; Shah, R.; Islam, R.; Asfani, D.A.; Nasution, T.H.; Abdillah, M.; Megantoro, P.; Krismanto, A.U. An Extreme Learning Machine Based Adaptive VISMA for Stability Enhancement of Renewable Rich Power Systems. *Electronics* **2022**, *11*, 247. [[CrossRef](#)]
3. Shankar, R.; Pradhan, S.; Chatterjee, K.; Mandal, R. A comprehensive state of the art literature survey on LFC mechanism for power system. *Renew. Sustain. Energy Rev.* **2017**, *76*, 1185–1207. [[CrossRef](#)]
4. Hamdy, A.; Kamel, S.; Nasrat, L.; Jurado, F. Frequency Stability of Two-Area Interconnected Power System with Doubly Fed Induction Generator Based Wind Turbine. In *Wide Area Power Systems Stability, Protection, and Security*; Springer: Berlin/Heidelberg, Germany, 2021; pp. 293–324.
5. Chen, G.; Li, Z.; Zhang, Z.; Li, S. An Improved ACO Algorithm Optimized Fuzzy PID Controller for Load Frequency Control in Multi Area Interconnected Power Systems. *IEEE Access* **2019**, *8*, 6429–6447. [[CrossRef](#)]
6. Akula, S.K.; Salehfar, H. Frequency Control in Microgrid Communities Using Neural Networks. In Proceedings of the 2019 North American Power Symposium (NAPS), IEEE, Wichita, KS, USA, 13–15 October 2019; pp. 1–6. [[CrossRef](#)]
7. Yousef, H. Adaptive fuzzy logic load frequency control of multi-area power system. *Int. J. Electr. Power Energy Syst.* **2015**, *68*, 384–395. [[CrossRef](#)]
8. Zhang, H.; Liu, J.; Xu, S. H-Infinity Load Frequency Control of Networked Power Systems via an Event-Triggered Scheme. *IEEE Trans. Ind. Electron.* **2019**, *67*, 7104–7113. [[CrossRef](#)]
9. Bevrani, H.; Feizi, M.R.; Atee, S. Robust Frequency Control in an Islanded Microgrid: H_∞ and μ -Synthesis Approaches. *IEEE Trans. Smart Grid* **2015**, *7*, 706–717. [[CrossRef](#)]
10. Das, S.K.; Rahman, M.; Paul, S.K.; Armin, M.; Roy, P.N.; Paul, N. High-Performance Robust Controller Design of Plug-In Hybrid Electric Vehicle for Frequency Regulation of Smart Grid Using Linear Matrix Inequality Approach. *IEEE Access* **2019**, *7*, 116911–116924. [[CrossRef](#)]
11. Rahman, M.; Sarkar, S.K.; Das, S.K.; Miao, Y. A comparative study of LQR, LQG, and integral LQG controller for frequency control of interconnected smart grid. In Proceedings of the 2017 3rd International Conference on Electrical Information and Communication Technology (EICT), Khulna, Bangladesh, 7–9 December 2017.
12. Moon, Y.H.; Ryu, H.S.; Kim, B.; Song, K.B. Optimal tracking approach to load frequency control in power systems. In Proceedings of the 2000 IEEE Power Engineering Society Winter Meeting, Conference Proceedings (Cat. No.00CH37077), Singapore, 23–27 January 2000; Volume 2, pp. 1371–1376.
13. Aoki, M. Control of large-scale dynamic systems by aggregation. *IEEE Trans. Autom. Control.* **1968**, *13*, 246–253. [[CrossRef](#)]
14. Topno, P.N.; Chanana, S. Load frequency control of a two-area multi-source power system using a tilt integral derivative controller. *J. Vib. Control* **2016**, *24*, 110–125. [[CrossRef](#)]
15. Gozde, H.; Taplamacioglu, M.C.; Kocaarslan, I. Comparative performance analysis of Artificial Bee Colony algorithm in automatic generation control for interconnected reheat thermal power system. *Int. J. Electr. Power Energy Syst.* **2012**, *42*, 167–178. [[CrossRef](#)]
16. Hasaniien, H.M.; El-Fergany, A.A. Salp swarm algorithm-based optimal load frequency control of hybrid renewable power systems with communication delay and excitation cross-coupling effect. *Electr. Power Syst. Res.* **2019**, *176*, 105938. [[CrossRef](#)]
17. Hasaniien, H.M. Whale optimisation algorithm for automatic generation control of interconnected modern power systems including renewable energy sources. *IET Gener. Transm. Distrib.* **2017**, *12*, 607–614. [[CrossRef](#)]
18. Nguyen, T.T.; Nguyen, T.T.; Duong, M.Q.; Doan, A.T. Optimal operation of transmission power networks by using improved stochastic fractal search algorithm. *Neural Comput. Appl.* **2020**, *32*, 9129–9164. [[CrossRef](#)]

19. Khadanga, R.K.; Kumar, A.; Panda, S. A novel sine augmented scaled sine cosine algorithm for frequency control issues of a hybrid distributed two-area power system. *Neural Comput. Appl.* **2021**, *33*, 12791–12804. [[CrossRef](#)]
20. Tepljakov, A.; Gonzalez, E.A.; Petlenkov, E.; Belikov, J.; Monje, C.A.; Petráš, I. Incorporation of fractional-order dynamics into an existing PI/PID DC motor control loop. *ISA Trans.* **2016**, *60*, 262–273. [[CrossRef](#)]
21. Tehrani, K.; Amirahmadi, A.; Rafiei, S.M.R.; Griva, G.; Barrandon, L.; Hamzaoui, M.; Rasoanarivo, I.; Sargos, F.M. Design of fractional order PID controller for boost converter based on Multi-Objective optimization. In Proceedings of the 14th International Power Electronics and Motion Control Conference EPE-PEMC 2010, T3-179–T3-185, Ohrid, Macedonia, 6–8 September 2010.
22. Abualigah, L.; Diabat, A.; Mirjalili, S.; Elaziz, M.A.; Gandomi, A.H. The Arithmetic Optimization Algorithm. *Comput. Methods Appl. Mech. Eng.* **2021**, *376*, 113609. [[CrossRef](#)]
23. Agushaka, J.O.; Ezugwu, A.E. Advanced arithmetic optimization algorithm for solving mechanical engineering design problems. *PLoS ONE* **2021**, *16*, e0255703. [[CrossRef](#)]
24. Azizi, M.; Talatahari, S. Improved arithmetic optimization algorithm for design optimization of fuzzy controllers in steel building structures with nonlinear behavior considering near fault ground motion effects. *Artif. Intell. Rev.* **2021**, 1–35. [[CrossRef](#)]
25. Wang, R.-B.; Wang, W.-F.; Xu, L.; Pan, J.-S.; Chu, S.-C. An Adaptive Parallel Arithmetic Optimization Algorithm for Robot Path Planning. *J. Adv. Transp.* **2021**, *2021*, 1–22. [[CrossRef](#)]
26. Guo, H.; Sun, Z.; Sun, H.; Ebrahimian, H. Optimal model of the combined cooling, heating, and power system by improved arithmetic optimization algorithm. *Energy Sources Part A Recover. Util. Environ. Eff.* **2021**, *41*, 1–23. [[CrossRef](#)]
27. Abualigah, L.; Diabat, A.; Sumari, P.; Gandomi, A. A Novel Evolutionary Arithmetic Optimization Algorithm for Multilevel Thresholding Segmentation of COVID-19 CT Images. *Processes* **2021**, *9*, 1155. [[CrossRef](#)]
28. Elkasem, A.H.A.; Khamies, M.; Magdy, G.; Taha, I.B.M.; Kamel, S. Frequency Stability of AC/DC Interconnected Power Systems with Wind Energy Using Arithmetic Optimization Algorithm-Based Fuzzy-PID Controller. *Sustainability* **2021**, *13*, 12095. [[CrossRef](#)]
29. Khamari, D.; Kumbhakar, B.; Patra, S.; A Laxmi, D.; Panigrahi, S. Load Frequency Control of a Single Area Power System using Firefly Algorithm. *Int. J. Eng. Res.* **2020**, *9*, 1318–1320. [[CrossRef](#)]
30. Sambariya, D.K.; Fagna, R. A robust PID controller for load frequency control of single area re-heat thermal power plant using elephant herding optimization techniques. In Proceedings of the 2017 International Conference on Information, Communication, Instrumentation and Control (ICICIC), Indore, India, 17–19 August 2017; pp. 1–6.
31. Hammid, A.T.; Hojabri, M.; Sulaiman, M.H.; Abdalla, A.N.; Kadhim, A.A. Load frequency control for hydropower plants using pid controller. *J. Telecommun. Electron. Comput. Eng.* **2016**, *8*, 47–51.
32. Dhanasekaran, B.; Siddhan, S.; Kaliannan, J. Ant colony optimization technique tuned controller for frequency regulation of single area nuclear power generating system. *Microprocess. Microsyst.* **2019**, *73*, 102953. [[CrossRef](#)]
33. Chao, D.; Chakraborty, P.; Nishikawa, T.; Motter, A.E. Hierarchical Power Flow Control in Smart Grids: Enhancing Rotor Angle and Frequency Stability with Demand-Side Flexibility. *IEEE Trans. Control Netw. Syst.* **2021**, *8*, 1046–1058. [[CrossRef](#)]
34. Elkasem, A.H.A.; Kamel, S.; Korashy, A.; Nasrat, L. Load Frequency Control Design of Two Area Interconnected Power System Using GWO. In Proceedings of the 2019 IEEE Conference on Power Electronics and Renewable Energy (CPERE), Aswan, Egypt, 23–25 October 2019; pp. 278–283.
35. Kamel, S.; Elkasem, A.H.A.; Korashy, A.; Ahmed, M.H. Sine Cosine Algorithm for Load Frequency Control Design of Two Area Interconnected Power System with DFIG Based Wind Turbine. In Proceedings of the 2019 International Conference on Computer, Control, Electrical, and Electronics Engineering (ICCCEEE), Khartoum, Sudan, 21–23 September 2019.
36. Ha, E.A.; Kamel, S.; Korashy, A.; Jurado, F. Application of Harris Hawks Algorithm for Frequency Response Enhancement of Two-Area Interconnected Power System with DFIG Based Wind Turbine. In Proceedings of the 2019 21st International Middle East Power Systems Conference (MEPCON), Cairo, Egypt, 17–19 December 2019; pp. 568–574.
37. Singh, S.P.; Prakash, T.; Singh, V.; Babu, M.G. Analytic hierarchy process based automatic generation control of multi-area interconnected power system using Jaya algorithm. *Eng. Appl. Artif. Intell.* **2017**, *60*, 35–44. [[CrossRef](#)]
38. El Yakine Kouba, N.; Mena, M.; Hasni, M.; Tehrani, K.; Boudour, M. A novel optimized fuzzy-PID controller in two-area power system with HVDC link connection. In Proceedings of the 2016 International Conference on Control, Decision and Information Technologies (CoDIT), St. Julian's, Malta, 6–8 April 2016; Volume 1, pp. 204–209.
39. Guha, D.; Roy, P.; Banerjee, S. Application of backtracking search algorithm in load frequency control of multi-area interconnected power system. *Ain Shams Eng. J.* **2018**, *9*, 257–276. [[CrossRef](#)]
40. Jagatheesan, K.; Anand, B.; Samanta, S.; Dey, N.; Santhi, V.; Ashour, A.S.; Balas, V.E. Application of flower pollination algorithm in load frequency control of multi-area interconnected power system with nonlinearity. *Neural Comput. Appl.* **2016**, *28*, 475–488. [[CrossRef](#)]
41. Padhan, D.G.; Majhi, S. A new control scheme for PID load frequency controller of single-area and multi-area power systems. *ISA Trans.* **2013**, *52*, 242–251. [[CrossRef](#)] [[PubMed](#)]
42. Guha, D.; Roy, P.; Banerjee, S. Load frequency control of interconnected power system using grey wolf optimization. *Swarm Evol. Comput.* **2016**, *27*, 97–115. [[CrossRef](#)]
43. Parmar, K.S.; Majhi, S.; Kothari, D. Load frequency control of a realistic power system with multi-source power generation. *Int. J. Electr. Power Energy Syst.* **2012**, *42*, 426–433. [[CrossRef](#)]

44. Khamies, M.; Magdy, G.; Ebeed, M.; Kamel, S. A robust PID controller based on linear quadratic gaussian approach for improving frequency stability of power systems considering renewables. *ISA Trans.* **2021**, *117*, 118–138. [[CrossRef](#)] [[PubMed](#)]
45. Li, X.; Hui, D.; Lai, X.; Yan, T. Power Quality Control in Wind/Fuel Cell/Battery/Hydrogen Electrolyzer Hybrid Micro-grid Power System. In *Applications and Experiences of Quality Control*; IntechOpen: London, UK, 2011. [[CrossRef](#)]
46. Yang, X.S.; Deb, S.; He, X. Eagle strategy with flower algorithm. In Proceedings of the 2013 International Conference on Advances in Computing, Communications and Informatics (ICACCI), Mysore, India, 22–25 August 2013; pp. 1213–1217.
47. Chen, Z.; Wu, L.; Lin, P.; Wu, Y.; Cheng, S. Parameters identification of photovoltaic models using hybrid adaptive Nelder-Mead simplex algorithm based on eagle strategy. *Appl. Energy* **2016**, *182*, 47–57. [[CrossRef](#)]
48. Ramadan, A.; Kamel, S.; Hassan, M.H.; Tostado-Véliz, M.; Eltamaly, A.M. Parameter Estimation of Static/Dynamic Photovoltaic Models Using a Developed Version of Eagle Strategy Gradient-Based Optimizer. *Sustainability* **2021**, *13*, 13053. [[CrossRef](#)]
49. Yapıcı, H.; Çetinkaya, N. An Improved Particle Swarm Optimization Algorithm Using Eagle Strategy for Power Loss Minimization. *Math. Probl. Eng.* **2017**, *2017*, 1063045. [[CrossRef](#)]
50. Santhosh, K.; Neela, R. Optimal Placement of Distribution Generation in Micro-Grid using Eagle Strategy with Particle Swarm Optimizer. *Int. J. Pure Appl. Math.* **2018**, *118*, 3819–3825.
51. Jin, H.; Lv, S.; Yang, Z.; Liu, Y. Eagle strategy using uniform mutation and modified whale optimization algorithm for QoS-aware cloud service composition. *Appl. Soft Comput.* **2021**, *114*, 108053. [[CrossRef](#)]
52. Podlubny, I. Fractional-order systems and PI/sup/spl lambda//D/sup/spl mu// -controllers. *IEEE Trans. Autom. Control* **1999**, *44*, 208–214. [[CrossRef](#)]
53. Podlubny, I.; Dorcak, L.; Kostial, I. On fractional derivatives, fractional-order dynamic systems and PI/sup/spl lambda//D/sup/spl mu// -controllers. In Proceedings of the 36th IEEE Conference on Decision and Control, San Diego, CA, USA, 12 December 1997; Volume 5, pp. 4985–4990.
54. Pan, I.; Das, S. Fractional Order AGC for Distributed Energy Resources Using Robust Optimization. *IEEE Trans. Smart Grid* **2015**, *7*, 2175–2186. [[CrossRef](#)]
55. Sondhi, S.; Hote, Y.V. Fractional order PID controller for load frequency control. *Energy Convers. Manag.* **2014**, *85*, 343–353. [[CrossRef](#)]
56. Mohanty, B.; Panda, S.; Hota, P.K. Controller parameters tuning of differential evolution algorithm and its application to load frequency control of multi-source power system. *Int. J. Electr. Power Energy Syst.* **2014**, *54*, 77–85. [[CrossRef](#)]
57. Mirjalili, S.; Mirjalili, S.M.; Lewis, A. Grey Wolf Optimizer. *Adv. Eng. Softw.* **2014**, *69*, 46–61. [[CrossRef](#)]
58. Kaur, S.; Awasthi, L.K.; Sangal, A.; Dhiman, G. Tunicate Swarm Algorithm: A new bio-inspired based metaheuristic paradigm for global optimization. *Eng. Appl. Artif. Intell.* **2020**, *90*, 103541. [[CrossRef](#)]
59. Dhiman, G.; Kumar, V. Seagull optimization algorithm: Theory and its applications for large-scale industrial engineering problems. *Knowl.-Based Syst.* **2018**, *165*, 169–196. [[CrossRef](#)]